



**SELF-ADAPTIVE PREDICTOR-CORRECTOR  
ALGORITHM FOR STATIC NONLINEAR  
STRUCTURAL ANALYSIS**

NASA-CR-165410  
19810024952

**Joseph Padovan**

April 1981

**Department of Mechanical Engineering  
The University of Akron  
Akron, Ohio 44325**

**LIBRARY COPY**

OCT 26 1981

LANGLEY RESEARCH CENTER  
LIBRARY, NASA  
HAMPTON, VIRGINIA

Prepared for  
LEWIS RESEARCH CENTER  
NATIONAL AERONAUTICS AND SPACE ADMINISTRATION  
CLEVELAND, OHIO 44315



NF01553

SELF-ADAPTIVE PREDICTOR-CORRECTOR  
ALGORITHM FOR STATIC NONLINEAR  
STRUCTURAL ANALYSIS

Joseph Padovan

April 1981

Department of Mechanical Engineering  
The University of Akron  
Akron, Ohio 44325

Prepared for  
Lewis Research Center  
National Aeronautics and Space Administration  
Cleveland, Ohio 44315

NASA Grant NAG3-54

1181-33495#

1. Report No. NASA CR 165410		2. Government Accession No.		3. Recipient's Catalog No.	
4. Title and Subtitle Self-Adaptive Predictor-Corrector Algorithms for Static Structural Analysis				5. Report Date April 1981	
				6. Performing Organization Code	
7. Author(s) J. Padovan				8. Performing Organization Report No.	
9. Performing Organization Name and Address The University of Akron Akron, OH 44325				10. Work Unit No.	
				11. Contract or Grant No. NAG 3-54	
12. Sponsoring Agency Name and Address National Aeronautics and Space Administration Washington DC 20546				13. Type of Report and Period Covered Interim	
				14. Sponsoring Agency Code	
15. Supplementary Notes Project Manager: C. C. Chamis Structures and Mechanical Technologies Division NASA Lewis Research Center Mail Stop 49-6 21000 Brookpark Road, Cleveland, OH 44135					
16. Abstract  A multi-phase self-adaptive predictor corrector type algorithm has been developed. This algorithm enables the solution of highly nonlinear structural responses including kinematic, kinetic and material effects as well as pre/post buckling behavior. The hierarchy of the strategy is such that three main phases are involved. The first features the use of a warpable hyperelliptic constraint surface which serves to upperbound dependent iterate excursions during successive Incremental Newton Raphson (INR) type iterations. The second corrector phase uses an energy constraint to scale the generation of successive iterates so as to maintain the appropriate form of local convergence behavior. The third involves the use of quality of convergence checks which enable various self-adaptive modifications of the algorithmic structure when necessary. Such restructuring is achieved by tightening various conditioning parameters as well as switch to different algorithmic levels so as to improve the convergence process. Results of several numerical experiments are included which illustrate the capabilities of the procedure to handle various types of static nonlinear structural behavior.					
17. Key Words (Suggested by Author(s)) nonlinear geometry, nonlinear material, post buckling, large deflections, numerical analysis			18. Distribution Statement  Unclassified, unlimited		
19. Security Classif. (of this report) Unclassified		20. Security Classif. (of this page) Unclassified		21. No. of Pages Approx. 75	
				22. Price*	

## ABSTRACT

This report describes a multi phase self-adaptive predictor corrector type algorithm. This type of algorithm enables the solution of highly nonlinear structural responses including kinematic, kinetic and material effects as well as potential pre/postbuckling behavior. The hierarchy of the strategy is such that three main phases are involved. The first features the use of a warpable hyperelliptic constraint surface which serves to upperbound dependent iterate excursions during successive Incremental Newton Raphson type iterations. The second corrector phase uses an energy constraint to scale the generation of successive iterates so as to maintain the appropriate form of local convergence behavior. The third involves the use of quality of convergence checks which enable various self-adaptive modifications of the algorithmic structure when necessary. Such restructuring is achieved by tightening various conditioning parameters as well as switch to different algorithmic levels so as to improve the convergence process. Several numerical experiments illustrate the capabilities of the procedure to handle varying types of nonlinear structural behavior.

## TABLE OF CONTENTS

Chapter		Page
1	INTRODUCTION	1
2	GOVERNING CLASSICAL INCREMENTAL NEWTON RAPHSON (INR) OPERATOR	4
	2.1 INR Algorithm	4
	2.2 Shortcomings	6
3	CONSTRAINED INR (CINR): PREDICTOR PHASE	7
	3.1 Hyper-Elliposidal Constraint Surface (HECS)	8
	3.2 Adaptive Warp of HECS	24
4	ENERGY CONSTRAINT: CORRECTOR PHASE	27
5	SUMMARY AND DISCUSSION OF NUMERICAL EXPERIMENTS	31
6	CONCLUSIONS	42
7	ACKNOWLEDGEMENT	46
8	REFERENCES	47
9	NOMENCLATURE	50

## TABLE OF FIGURE CAPTIONS

<u>Fig. No.</u>	<u>Caption</u>	<u>Page No.</u>
1	Curvature initiated adaptive updating of HECS	10
2	Iterative process associated with HECS Constrained MINR algorithm in zone of MDPD curvature	11
3	Nonmonotone but convergent iterative process associated with HECS constrained MINR algorithm in zone of MIPD curvature	16
4	Nonmonotone but convergent iterative process associated with HECS constrained MINR algorithm in zone of MDID curvature	18
5	Monotone iterative process associated with HECS constrained MINR algorithm in zone of MIPD curvature	19
6	Iterative process associated with turning point without updating	22
7	Iterative process associated with turning point with updating	23
8	FE simulation of rubber sheet	35
9	Load deflection curve of rubber sheet	36
10	Strain energy space of rubber sheet	37
11	FE simulation of spherical cap	39
12	Load deflection curve of spherical cap	40
13	Strain energy space of spherical cap	41
14	FE simulation of arch	43
15	Load deflection curve of arch	44
16	Strain energy space of arch	45

## 1. INTRODUCTION

One of the central features in the development of finite element computer programs for nonlinear analysis is the proper selection of solution algorithms. The nature of structural nonlinearities is generally quite diverse when both kinematic and material effects are included. Specifically, for static problems, such effects give rise to nonlinear algebraic equations which may possess path dependent multiple solutions. In this context, the quest for reliable as well as computationally efficient solutions to such problems is a very demanding task.

Solution procedures for nonlinear problems have been discussed by a multitude of authors [1-12]. In this direction, the mature works of Bergan et al. [9], Riks [10] and Crisfield [11, 12] give a good overview of much of the progress made to date. As can be seen from these papers [9-12], unlike linear problems, it is extremely difficult to develop a single methodology of general validity which can be used to handle the diversity of potential structural problems. Since the formulation of the problem and hence the associated computer coding architecture is strongly dependent on the algorithmic approach taken, generally most general purpose (GP) nonlinear finite element (FE) codes have adopted one particular methodology through which the nonlinear problem is solved [13-14]. In this context, generally some variant of the Incremental Newton Raphson (INR) approach has been chosen [13-15]. While the INR procedure is perhaps the most powerful of the iterative solution techniques, it is subject to several short-

comings. The more important of these can be categorized as follows:

- 1) Inefficiencies associated with update requirements; and
- 2) Sensitivities/anomalous convergence characteristics in the neighborhood of turning points (zones of changing curvature definiteness), bifurcations, "shallow" curvature, snap through behavior, etc.

While the recently advocated pseudo update procedures [16-18] provide a partial answer to the computational inefficiencies associated with updating, no real improvement is achieved in category 2) problems nor is it clear what happens in path dependent and/or multiple solution situations.

To overcome the sensitivities associated with the use of the INR algorithm in the vicinity of turning points several approaches have been advocated, in particular:

- a) Use of deflection control [19];
- b) Rotation of solution space via introduction of auxiliary stiffness [20];
- c) Switch from step-iterative to pure Euler-Cauchy type incrementations initiated via curvature monitoring [9]; and
- d) Use of constraints to control successive dependent iterate excursions [10-12].

Since the main sensitivities/anomalous behavior of the INR type algorithms appears to be the generation of excessive iterate excursions in neighborhoods of turning point, shallow curvature etc., the constrained approach advocated by d) [10-12] appears to be the best choice for use in general purpose (GP) codes.



The difficulty of the foregoing approaches lies in the fact that there is no automatic correction features associated with the algorithms wherein, as the solution proceeds, its quality<sup>[14]</sup> is monitored so as to enable the appropriate automatic corrective action to be taken. In this context, this report develops a self-adaptive type predictor-corrector algorithmic strategy. The hierarchy of the strategy is such that the predictor phase consists of a constrained type INR algorithm (CINR) which is employed to tunnel into the solution space. It features the use of a warpable hyperelliptic constraint surface (HECS), which serves to upperbound dependent iterate excursions during successive iterations. The second corrector phase of the solution strategy lies in the use of an energy constraint to scale the generation of successive iterates so as to maintain the appropriate form of convergence behavior (monotone, oscillating, etc.) associated with the type of curvature of the zone of solution space wherein the algorithmic tunneling is taking place. The third phase of the solution hierarchy involves the use of quality/convergence checks<sup>[14]</sup> which enable various self-adaptive modifications of the algorithmic structure.

In the sections which follow, detailed discussions are given on the classical INR algorithm and its limitations, the development of the various levels of the self adaptive predictor-corrector approach as well as the results of several numerical examples which demonstrate the capabilities of the new procedure.

## 2. GOVERNING CLASSICAL INR OPERATOR

Before overviewing the development of the CINR algorithm, it is worthwhile to review the salient features of the INR as well as outline several of its more important shortcomings.

### 2.1 INR Algorithm

Assuming that large deformation processes are in effect, the virtual work principle takes the following form in Lagrangian coordinates namely<sup>[21]</sup>

$$\int_R (\delta L_{ij} S_{ij} + \delta u_i Q_i) dv = 0 \quad (2.1)$$

where  $\delta( )$ ,  $S_{ij}$ ,  $L_{ij}$ ,  $U_i$ ,  $Q_i$  and  $R$  respectively denote the variational operator, 2nd Piola-Kirchhoff stress tensor <sup>[21]</sup>, the Lagrangian (Green's) strain tensor <sup>[21]</sup>, displacement, body force and lastly the region occupied by the structure. Introducing the shape function description of displacements<sup>[15]</sup>,

$$\underline{U} = [N]\underline{Y} \quad (2.2)$$

the following assembled finite element (FE) formulation is obtained, that is

$$\int_R [B^*(\underline{Y})]^T \underline{S} dv = \underline{F}(\underline{Y}). \quad (2.3)$$

where  $( )^T$  is matrix transposition, and

$$[B^*] = [B] + [B_n(\underline{Y})][G] \quad (2.4)$$

such that  $[B]$ ,  $[B_n]$ ,  $[G]$  are nonlinear partitions of the strain and  $[N]$ ,  $\underline{S}$  and  $\underline{Y}$  respectively represent the shape function, vector form of stress tensor and the nodal displacements.

Since (2.3) is inherently nonlinear, assuming that the material properties can be cast in a tangent stiffness formulation, namely

$$d\tilde{S} \sim [D_T][B^*]d\tilde{Y} \quad (2.5)$$

then (2.3) can be expanded into a truncated Taylor series to yield the following operator:

$$\Delta F(\tilde{Y}) \sim [K_T(\tilde{Y})]\Delta\tilde{Y} + O(\tilde{Y}^T\tilde{Y}) \quad (2.6)$$

Now, expressing (2.6) and (2.3) in algorithmic form yields the following INR operator, that is

$$\Delta Y_{\ell}^i = [K_T(Y_{\ell}^j)]^{-1} \{ \tilde{F}_{\ell} - \int_R [B^*(Y_{\ell}^{i-1})]^T \tilde{S}(Y_{\ell}^{i-1}) \} \quad (2.7)$$

where  $\ell$ ,  $i$ ,  $j$ ,  $[\ ]^{-1}$ ,  $\Delta Y_{\ell}^i$ ,  $Y_{\ell}^i$  and  $\tilde{F}_{\ell}$  respectively denote the  $\ell$ th loadstep,  $i$ th iteration,  $j$ th intermittent update of the stiffness, matrix inverse,  $i$ th displacement increment of the  $\ell$ th loadstep and lastly the total nodal displacement and force associated with  $\ell$ th loadstep.

The convergence criteria typically associated with (2.7) involve normed checks of successive displacement increments and nodal force imbalances, that is [9, 22]

$$\frac{||\Delta Y_{\ell}^i - \Delta Y_{\ell}^{i-1}||_1}{||\Delta Y_{\ell}^i||_1} < \text{tol} \quad (2.8)$$

$$\frac{||\tilde{F}_{\ell} - \tilde{F}(Y_{\ell}^i)||_1 - ||\tilde{F}_{\ell} - \tilde{F}(Y_{\ell}^{i-1})||_1}{||\tilde{F}_{\ell} - \tilde{F}(Y_{\ell}^i)||_1} < \text{tol} \quad (2.9)$$

where here  $||\cdot||_1$  designates the norm

$$||Y_{\ell}||_1 = \sum_{i=1}^n |Y_{\ell i}| \quad (2.10)$$

Most typically, satisfaction of such criteria from increment to increment is said to be sufficient to guarantee a convergent solution.

To streamline the use of (2.8), the consensus opinion seems to advocate that  $[K_T]$  be updated and inverted only at the beginning of a loadstep<sup>[9, 22]</sup>. This approach yields the so-called modified INR (MINR) operator. As noted earlier, to improve the accuracy/convergence characteristics of such an approach, numerous pseudo updates have recently been advocated. Here the BFGS family of updates has figured prominently<sup>[16-18]</sup>.

## 2.2 Shortcomings

While the modified, intermittantly /constantly/pseudo (BFGS)<sup>[16-18]</sup> updated versions of the INR algorithm converge quadratically if the load increments are sufficiently "small", several shortcomings can occur when such is not the case. Additional difficulties are also encountered in zones of shallow or changing curvature definiteness. This situation can be summarized by the following comments:

- i) There is no direct way of preselecting increment size as nodal force - deflection space changes curvature;
- ii) There is no direct way of establishing an upper bound on the magnitude of the iterated displacement, strain, stress and energy excursions for a given load increment;
- iii) Excessive iterate excursions inherently occur in the neighborhood of "shallow" slope zones of the force - displacement space, and;

iv) Without intermittent or constant updating, the iterated version of the MINR can exhibit nonmonotone potentially divergent convergence characteristics for monotone increasing/decreasing, positive/negative definite solution curvatures. [14]

The excessive iterated dependent variable excursions noted above tend to cause drifting from the solution curve. When such drift is sufficiently large, depending on the topology of the solution space, rather strong nonmonotone type divergence may be initiated as the iteration process continues [14].

### 3. CONSTRAINED INR (CINR): PREDICTOR PHASE

In the context of the remarks made in the previous section, it follows that one way to limit the excessive excursions of successive iterates is to establish some form of upper bound constraint. Riks<sup>[10]</sup> first considered this approach by developing a methodology which features the INR and a special parameter controlling the progress of the computation in nodal force-deflection space. In geometrical terms, the control parameter selected corresponds approximately to the arc length of the equilibrium path to be computed. It is introduced into the governing field equations. Hence, for a problem with  $N$  displacement variables, the addition of the constraint equation yields an  $N + 1$  dimensional space the solution to which is obtained by the NR method.

Due to the manner in which Riks<sup>[10]</sup> casts his constraint equation, its direct use with the equilibrium equations tends to be somewhat awkward for direct use with the standard FE methodology.

To circumvent this difficulty, Crisfield [11,12] employed the technique advocated by Batoz and Dhatt [19] for standard displacement control. Using such an approach, Crisfield [11,12] recast the out of balance force vector as a parametrized function of the external load vector. Due to the use of an inner product type constraint on the allowable displacement iterate excursions, this approach enabled the development of an expression which sizes the allowable iterative changes in external loading.

In the subsections to follow, the constrained approach is generalized to a more comprehensive and self-adaptive form. This will be partly achieved by introducing a more general constraint namely the hyper-elliptic constraint surface (HECS). Because of the greater adaptability of the HECS, this will enable the CINR to act as a refined self-adaptive predictor algorithm. In this context, the resulting algorithmic structure will be left flexible enough so that in the next section, an energy constraint can be introduced to serve in the capacity of the associated corrector algorithm.

### 3.1 Hyper-Ellipsoidal Constraint

#### Surface HECS

As noted earlier, to extend the versatility and adaptability of the CINR approach, this paper introduces a more general constraint condition namely the hyper-elliptic constraint surface HECS as defined by the expression

$$\mu_k (||\underline{y}_k||_2)^2 + (||\underline{f}_k||_2)^2 = (||\Delta \underline{F}_k||_2)^2 \quad (3.1)$$

where  $||\bullet||_2$  designates the Euclidean norm and

$$||\underline{y}_\ell||_2 = (\sum_i y_{\ell i}^2)^{1/2} \quad (3.2)$$

such that referring to Fig. (1),  $\mu_\ell$  is a warping parameter which together with the load increment  $\Delta F_\ell$  defines the curvature/geometry of the HECS, while  $\underline{y}_\ell$  and  $\underline{f}_\ell$  are respectively the displacement and load excursions relative to the starting point of the given load increment. Figure 2 schematically illustrates the successive use of (3.1) in conjunction with the MINR algorithm. By tying the selection of  $\mu_\ell$  to the local curvature of the solution curve, the geometry of the HECS can be adaptively updated to improve the solution flow. As can be seen from Fig. (2), the HECS itself establishes a greatest upper bound possible by the iterative excursions of the dependent field variables. In particular, for the nodal displacements, the maximum allowable excursion for a given load increment is defined by the expression

$$||\underline{y}_\ell||_2 \leq ||\Delta F_\ell||_2 / \sqrt{\mu_\ell} \quad (3.3)$$

By adjusting  $\Delta F_\ell$  and/or  $\mu_\ell$ , varying bounds can be developed for the incremental nodal displacement excursions  $\underline{y}_\ell$ .

To establish the requisite algorithmic hardware arising from the use of the HECS, it follows that outside of turning points and bifurcations, there are basically four types of curvature behavior associated with the solution curve namely:

- i) Monotone decreasing and positive definite (MDPD);
- ii) Monotone increasing and positive definite (MIPD);
- iii) Monotone decreasing and indefinite (MDID); and
- iv) Monotone increasing and indefinite (MIID)

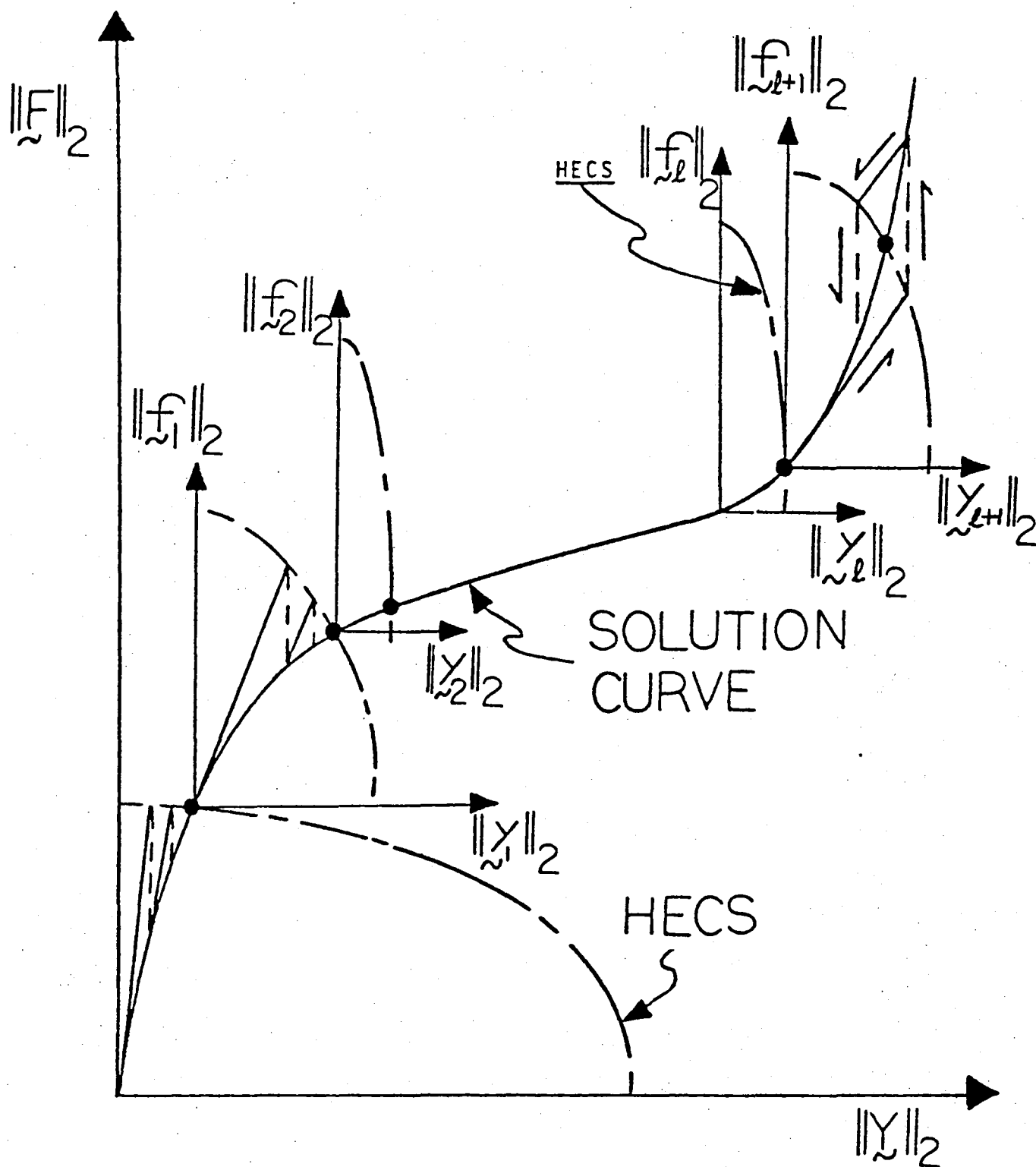


FIG.1 Curvature initiated adaptive updating of HECS



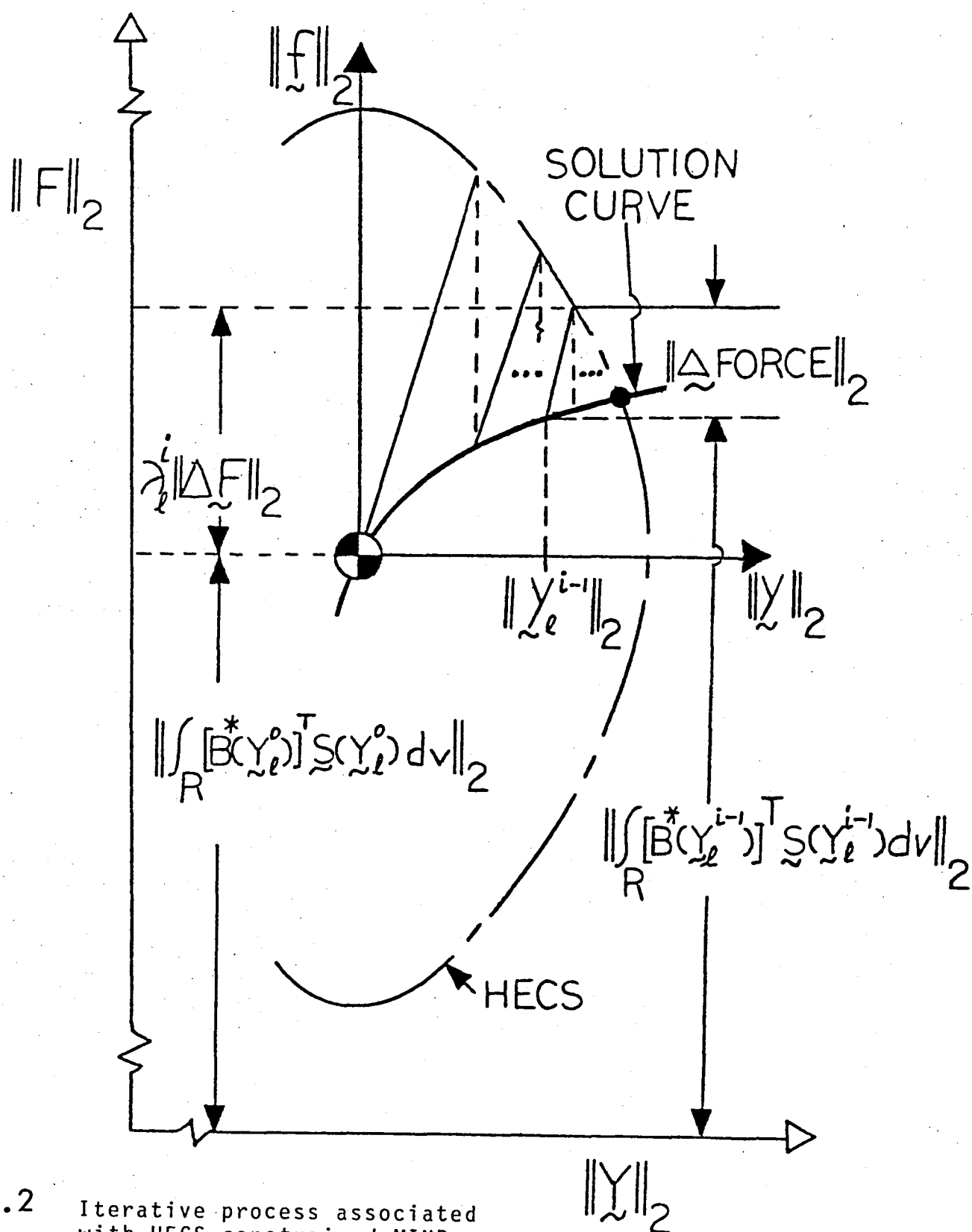


FIG.2 Iterative process associated with HECS constrained MINR algorithm in zone of MDPD curvature

Since each places varying demands on the algorithmic apparatus, the CINR involving the HECS will be structured to admit all such situations.

A structure generally exhibits MDPD behavior at the outset. This case will be used as the starting point of the development. Referring to Fig. (2), it follows that using the multidimensional starting point of the  $\ell^{\text{th}}$  increment as a local origin of the HECS, we have that

$$\begin{aligned}\tilde{y}_{\ell}^i &= \tilde{y}_{\ell}^i - \tilde{y}_{\ell}^0 \\ &= \tilde{y}_{\ell}^{i-1} - \tilde{y}_{\ell}^0 + \Delta \tilde{y}_{\ell}^i\end{aligned}\quad (3.4)$$

where for the  $i^{\text{th}}$  iteration

$$\Delta \tilde{y}_{\ell}^i = \tilde{y}_{\ell}^i - \tilde{y}_{\ell}^{i-1} \quad (3.5)$$

Similarly,  $\tilde{f}_{\ell}^i$  is given by

$$\tilde{f}_{\ell}^i = \lambda_{\ell}^i \Delta F_{\ell} \quad (3.6)$$

where  $\lambda_{\ell}^i$  denotes the incremental loading parameter which is iteratively adjusted until the intersection point of the HECS and the solution curve is achieved for the given load increment.

To start the process, either the MINR, INR, or pseudo INR algorithms are used to project the solution curve so as to determine its intersection with the HECS. In terms of the modified NR strategy defined in Fig. (2), the driving force potential enabling this calculation is given by

$$\Delta \text{force} = \lambda_{\ell}^i \Delta F_{\ell} - \int_R \{ [B^*(\tilde{y}_{\ell}^{i-1})] \tilde{S}(\tilde{y}_{\ell}^{i-1}) - [B^*(\tilde{y}_{\ell}^0)]^T \tilde{S}(\tilde{y}_{\ell}^0) \} dv \quad (3.7)$$

Hence, considering the MINR for the moment,

$$\Delta \underline{Y}_\ell^i = [\underline{K}_T(\underline{Y}_\ell^0)]^{-1} (\lambda_\ell^i \Delta \underline{F}_\ell - \int_R \{ [\underline{B}^*(\underline{Y}_\ell^{i-1})]^T \underline{S}(\underline{Y}_\ell^{i-1}) - [\underline{B}^*(\underline{Y}_\ell^0)]^T \underline{S}(\underline{Y}_\ell^0) \} dv) \quad (3.8)$$

where  $[\underline{K}_T]$  is updated only at the beginning of the load increment.

Employing (3.8), (3.4) can be reduced to the form

$$\underline{Y}_\ell^i = \underline{a}_\ell^{i-1} + \lambda_\ell^i \underline{b}_\ell \quad (3.9)$$

where here

$$\underline{a}_\ell^{i-1} = \underline{Y}_\ell^{i-1} - \underline{Y}_\ell^0 - [\underline{K}_T(\underline{Y}_\ell^0)]^{-1} \int_R \{ [\underline{B}^*(\underline{Y}_\ell^{i-1})]^T \underline{S}(\underline{Y}_\ell^{i-1}) - [\underline{B}^*(\underline{Y}_\ell^0)]^T \underline{S}(\underline{Y}_\ell^0) \} dv \quad (3.10)$$

$$\underline{b}_\ell = [\underline{K}_T(\underline{Y}_\ell^0)]^{-1} \Delta \underline{F}_\ell \quad (3.11)$$

To obtain the intersection point, substituting (3.6) and (3.9) into the relation defining the HECS namely (3.1), the following expression is obtained

$$\mu_\ell (||\underline{a}_\ell^{i-1} + \lambda_\ell^i \underline{b}_\ell||_2)^2 + ((\lambda_\ell^i)^2 - 1)(||\Delta \underline{F}_\ell||_2)^2 = 0 \quad (3.12)$$

Solving (3.12) for the  $\ell^{\text{th}}$  incremental loading parameter  $\lambda_\ell^i$  yields

$$\lambda_\ell^i = \frac{1}{2\Xi_{\ell 1}^{i-1}} \{ -\Xi_{\ell 2}^{i-1} \pm [(\Xi_{\ell 2}^{i-1})^2 - 4\Xi_{\ell 1}^{i-1}\Xi_{\ell 3}^{i-1}]^{1/2} \} \quad (3.13)$$

where here

$$\Xi_{\ell 1}^{i-1} = (||\underline{b}_\ell||_2)^2 \mu_\ell + (||\Delta \underline{F}_\ell||_2)^2 \quad (3.14)$$

$$\Xi_{\ell 2}^{i-1} = \mu_{\ell} (\underline{b}_{\ell}^T \underline{a}_{\ell}^{i-1} + (\underline{a}_{\ell}^{i-1})^T \underline{b}_{\ell}) \quad (3.15)$$

$$\Xi_{\ell 3}^{i-1} = \mu_{\ell} (\|\underline{a}_{\ell}^{i-1}\|_2^2 - \|\Delta \underline{F}_{\ell}\|_2^2) \quad (3.16)$$

The proper sign appearing in (3.13) is chosen by noting that for MDPD curvature, the bilinear forms  $\Xi_{\ell k}^{i-1}$ ;  $k = 1, 2, 3$  have the following types of definiteness namely

$$\left. \begin{aligned} (\Xi_{\ell 1}^{i-1}; \Xi_{\ell 2}^{i-1}) &> 0 \\ \Xi_{\ell 3}^{i-1} &\leq 0 \end{aligned} \right\} \quad i = 1, 2, \dots \quad (3.17)$$

Here since  $\lambda_{\ell}^i$  must itself be positive definite for MDPD solution geometries, (3.13) is chosen to take the form

$$\lambda_{\ell}^i = \frac{1}{2\Xi_{\ell 1}^{i-1}} \{-\Xi_{\ell 2}^{i-1} + [(\Xi_{\ell 2}^{i-1})^2 - 4\Xi_{\ell 1}^{i-1} \Xi_{\ell 3}^{i-1}]^{1/2}\} \quad (3.18)$$

In this context, the CMINR is structured as follows

$$\begin{aligned} \Delta \underline{Y}_{\ell}^i = & [\underline{K}_T(\underline{Y}_{\ell}^0)]^{-1} \left( \frac{\Delta \underline{F}}{2\Xi_{\ell 1}^{i-1}} \{-\Xi_{\ell 2}^{i-1} + [(\Xi_{\ell 2}^{i-1})^2 - 4\Xi_{\ell 1}^{i-1} \Xi_{\ell 3}^{i-1}]^{1/2}\} - \right. \\ & \left. \int_R ([\underline{B}^*(\underline{Y}_{\ell}^{i-1})]^T \underline{S}(\underline{Y}_{\ell}^{i-1}) - [\underline{B}^*(\underline{Y}_{\ell}^0)]^T \underline{S}(\underline{Y}_{\ell}^0)) d\underline{v} \right) \quad (3.19) \end{aligned}$$

Note for MDPD solution curves, the sequence of successive  $\Delta \underline{Y}_{\ell}^i$  iterates are themselves positive definite. Contingent on the successful satisfaction of the convergence criteria, the global external load takes the form

$$\underline{F}_{\ell} = \underline{F}_{\ell-1} + \lambda_{\ell}^I \Delta \underline{F}_{\ell} \quad (3.20)$$

where  $I$  denotes the last iteration count.

Because of the foregoing properties, successive iterates associated with MDPD portions of the solution curve remain confined inside the HECS. Such is not the case for MIPD situations. As seen in Fig. 3, nonmonotone oscillatory convergence is achieved wherein successive iterates alternate between increasingly closer inside and outside positions relative to the multidimensional intersection of the HECS and the solution curve.

While the CMINR algorithm defined by (3.19) also applies here, since the convergence/quality checks [14] used to monitor the state of solution development may be keyed in on monotonicity properties, it is important to determine the "in/outsideness" of successive iterates. This enables the determination of a consistent convergence process. To check for such properties, the functional characteristics of the HECS can be used to establish the in/outsideness of the  $i^{\text{th}}$  iterate by evaluations of the following condition flag namely

$$\phi_{\ell}^i = \mu_{\ell} (||\tilde{y}_{\ell}^i||_2)^2 + (||\tilde{f}_{\ell}^i||_2)^2 - (||\Delta \tilde{F}_{\ell}||_2)^2 \quad (3.21)$$

where

$$\phi_{\ell}^i \begin{cases} > 0 & \text{outside point} \\ < 0 & \text{inside point} \end{cases} \quad (3.22)$$

Note for such situations, the definiteness characteristics of  $\Xi_{\ell k}^i$ ;  $k = 1, 2, 3$  are altered. In particular, since the successive solution curvatures are steeper than the initial state, it follows that

$$\left. \begin{array}{l} \Xi_{\ell 1}^{i-1} > 0; \Xi_{\ell 2}^{i-1} < 0 \\ \Xi_{\ell 3}^{i-1} \text{ indefinite} \end{array} \right\} i = 1, 2, 3 \dots \quad (3.23)$$

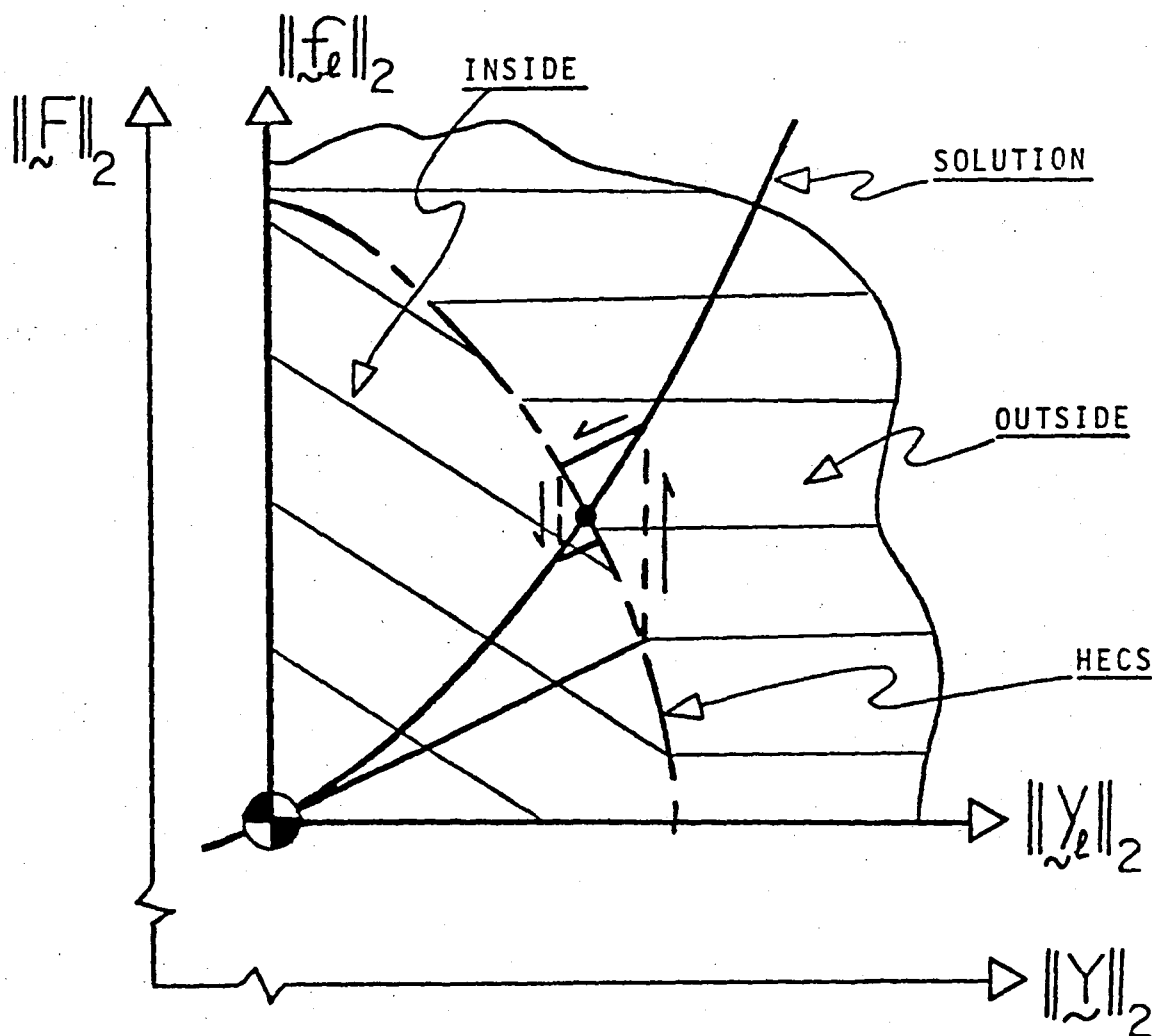


FIG.3 Nonmonotone but convergent iterative process associated with HECS constrained MINR algorithm in zone of MIPD curvature

In the case of MDID local solution behavior, the bilinear forms  $\Xi_k^{i-1}$ ;  $k = 1, 2, 3$  have the following definiteness characteristics for  $\forall i$  namely

$$\left. \begin{array}{l} \Xi_{\ell 1}^{i-1} > 0; \Xi_{\ell 2}^{i-1} < 0 \\ \Xi_{\ell 3}^{i-1} \text{ indefinite} \end{array} \right\} i = 1, 2, 3, \dots \quad (3.24)$$

Note, in the context of Fig. (4), the force potential driving the INR projection of the solution curve into its intersection with the HECS is given by the same expression as positive definite situations, namely (3.8). Here though, due to the nature of the intersection, the load parameter takes the form

$$\lambda_{\ell}^i = \frac{1}{\Xi_{\ell 1}^{i-1}} \left\{ -\Xi_{\ell 2}^{i-1} - [(\Xi_{\ell 2}^{i-1})^2 - 4\Xi_{\ell 1}^{i-1} \Xi_{\ell 3}^{i-1}]^{1/2} \right\} \quad (3.25)$$

Note as with MIPD situations, successive iterates form an oscillatory nonmonotone sequence whose members are alternating inside or outside of the HECS. Such properties can be ascertained by employing the criterion function defined by (3.21).

Lastly for MIID situations described in Fig. (5), all the modified algorithms established for the preceeding indefinite case also apply here; the only exception being that successive iterates display a MDID type behavior and hence remain inside the HECS. In this context,

$$\left. \begin{array}{l} (\Xi_{\ell 1}^{i-1}, \Xi_{\ell 2}^{i-1}) > 0 \\ \Xi_{\ell 3}^{i-1} \leq 0 \end{array} \right\} i = 1, 2, \dots, I \quad (3.26)$$

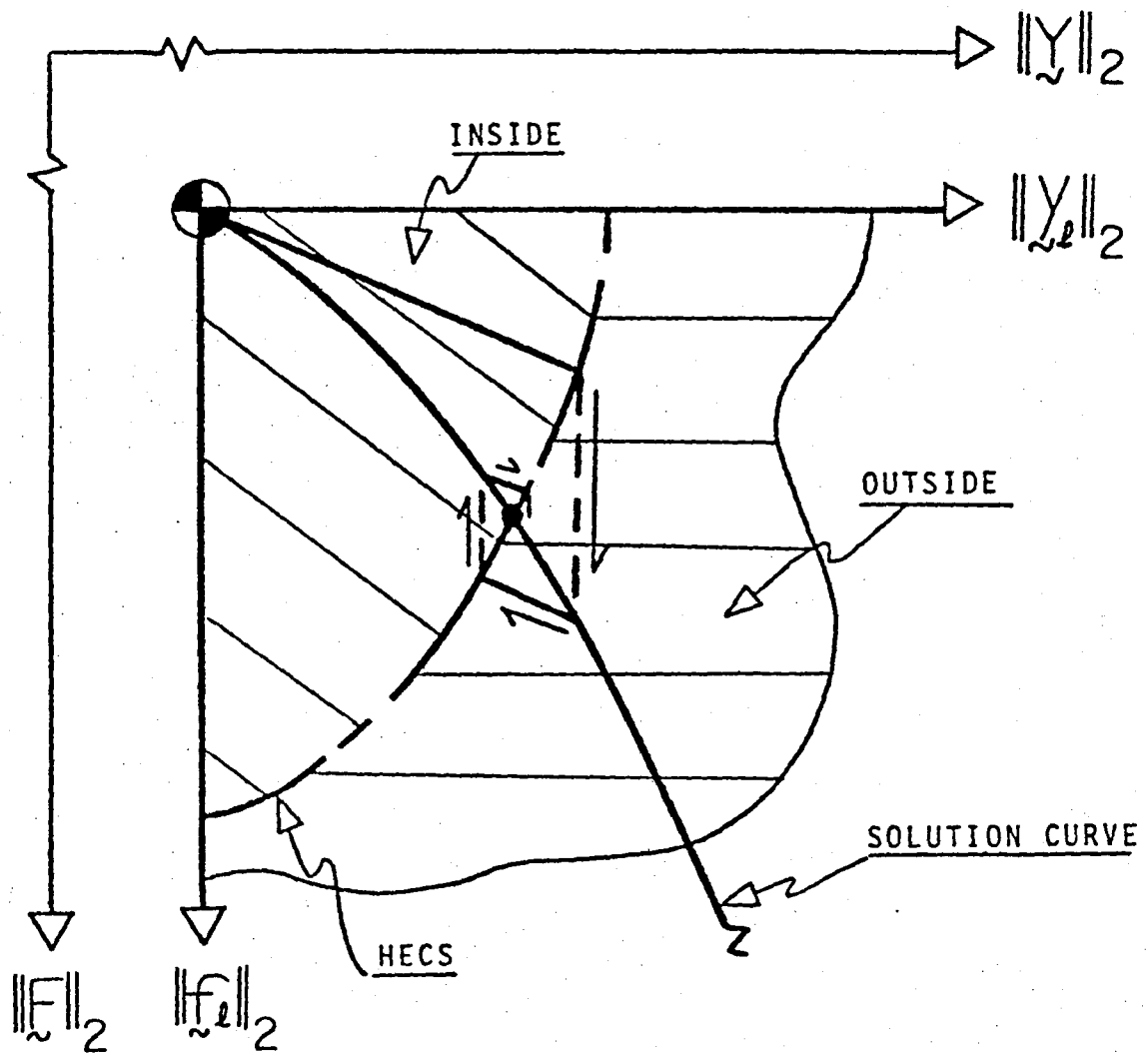


FIG. 4 Nonmonotone but convergent iterative process associated with HECS constrained MINR algorithm in zone of MDID curvature



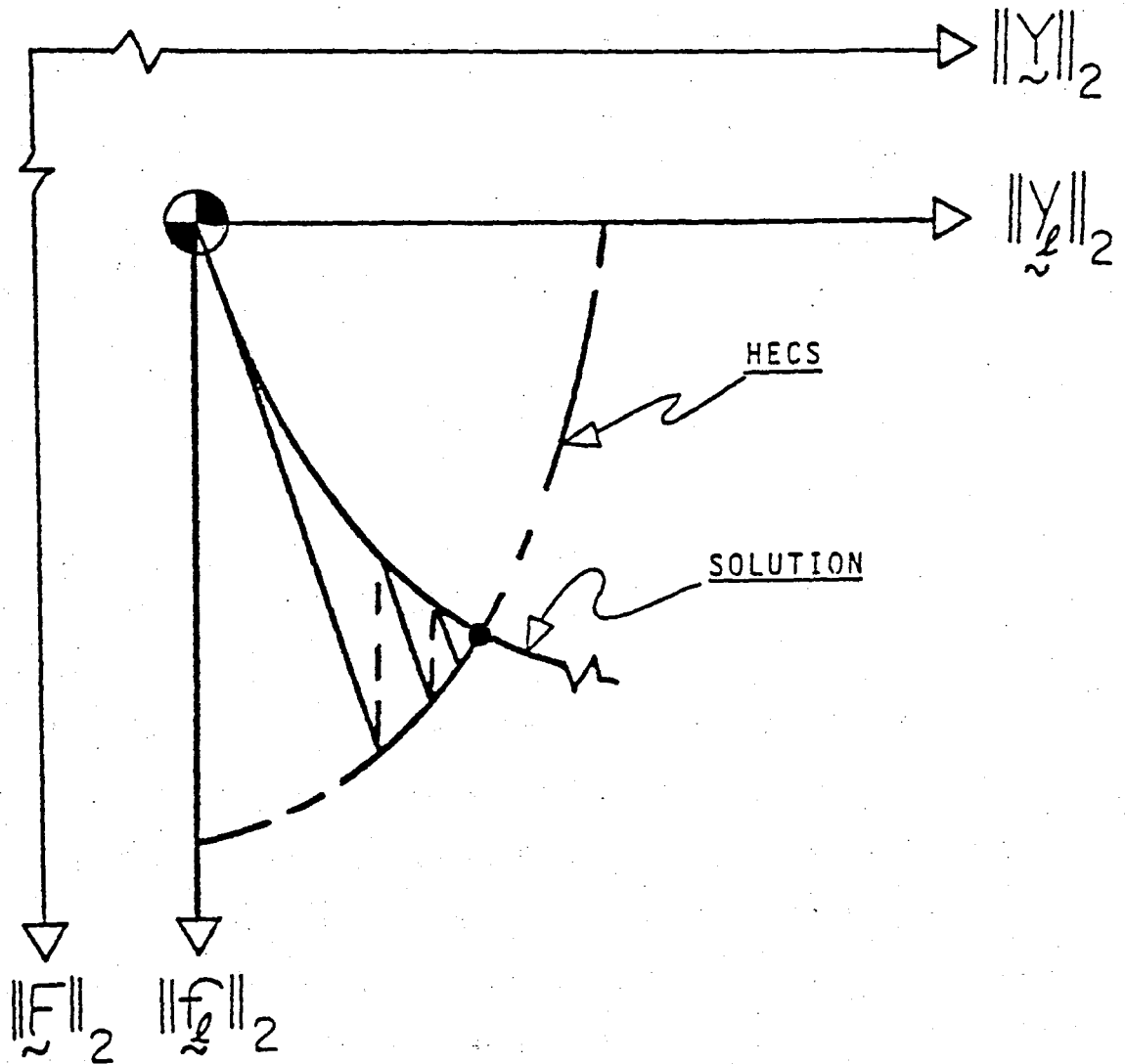


FIG. 5 Monotone iterative process associated with HECS constrained MINR algorithm in zone of MIPD curvature

The preceeding algorithms were all developed for some general  $i^{\text{th}}$  iteration. For the first, several simplifications can obviously be made, in particular the load parameter takes the form

$$\lambda_{\ell}^i = \pm \left[ \frac{(\|\Delta F_{\ell}\|_2)^2}{\mu_{\ell}(\|\tilde{b}_{\ell}\|_2)^2 + (\|\Delta F_{\ell}\|_2)^2} \right]^{1/2} \quad (3.27)$$

In terms of (3.27), the algorithm defining the successive displacement iterates for PD and ID situations reduce to the following form namely

$$\Delta Y_{\ell}^1 = [K_T(Y_{\ell}^0)]^{-1} \left[ \frac{(\|\Delta F_{\ell}\|_2)^2}{\mu_{\ell}(\|\tilde{b}_{\ell}\|_2)^2 + (\|\Delta F_{\ell}\|_2)^2} \right]^{1/2} \quad (3.28)$$

$$\Delta Y_{\ell}^1 = - [K_T(Y_{\ell}^0)]^{-1} \left[ \frac{(\|\Delta F_{\ell}\|_2)^2}{\mu_{\ell}(\|\tilde{b}_{\ell}\|_2)^2 + (\|\Delta F_{\ell}\|_2)^2} \right]^{1/2} \quad (3.29)$$

In the preceeding algorithmic developments, it was tacitly assumed that the types of definiteness of the solution curve remained unchanged during the successive iterations associated with a given load increment. For situations which straddle turning points, such is not the case. Since the algorithmic structure is different for positive and negative definite situations, some provisions must be developed to identify such changes in definiteness so that the proper modifications can be made. To initiate adaptive updates of the stiffness as triggered by definiteness changes, it is assumed that load incrementing as enforced by the HECS is tight enough so that either MDPD or MIID behavior is

encountered to the left of turning points. For such situations, comparison checks between successive iterates can be used to monitor definiteness changes. In this context, accounting for the initial curvature of a given load increment, the following condition flag can be introduced and monitored namely

$$K_u^{\ell i} = \text{sgn}(C_R^\ell) \text{sgn}(\|F_{\ell}^{i-1}\|_2 - \|F_{\ell}^{i-2}\|_2) \quad (3.30)$$

where plus to minus sign change can be used to signal updates.

In the context of (3.30), the algorithm defining  $\lambda_\ell^i$  takes the form

$$\lambda_\ell^i = \frac{1}{2\varepsilon_{\ell 1}^{i-1}} \left\{ -\varepsilon_{\ell 2}^{i-1} + K_u^{\ell i} [(\varepsilon_{\ell 2}^{i-1})^2 - 4\varepsilon_{\ell 2}^{i-1} \varepsilon_{\ell 3}^{i-1}]^{1/2} \right\} \quad (3.31)$$

$i > 1$

An alternative test can be used to trigger the updating of the stiffness in the neighborhood of turning points. As seen from Fig. (6), successive  $\lambda_\ell^i$  form a monotone decreasing sequence namely

$$\lambda^0 > \lambda_\ell^1 > \lambda_\ell^2 > \dots > \lambda_\ell > \dots \quad (3.32)$$

While such behavior may initially occur, as seen from Fig. (7), passed a certain point, successive  $\lambda_\ell^i$  values can become negative definite namely

$$\lambda_\ell^0 > \lambda_\ell^1 > \dots > \lambda_\ell^{i-1} > 0 > \lambda_\ell^i > \dots \quad (3.33)$$

Such a change in definiteness can be used to trigger the update process. At such a point, the choice of the proper  $\lambda_\ell^i$  algorithm is keyed in on the definiteness encountered. As an example, for turning points which involve transitions from negative to positive definite curvature, the monotonicity noted above is reversed.

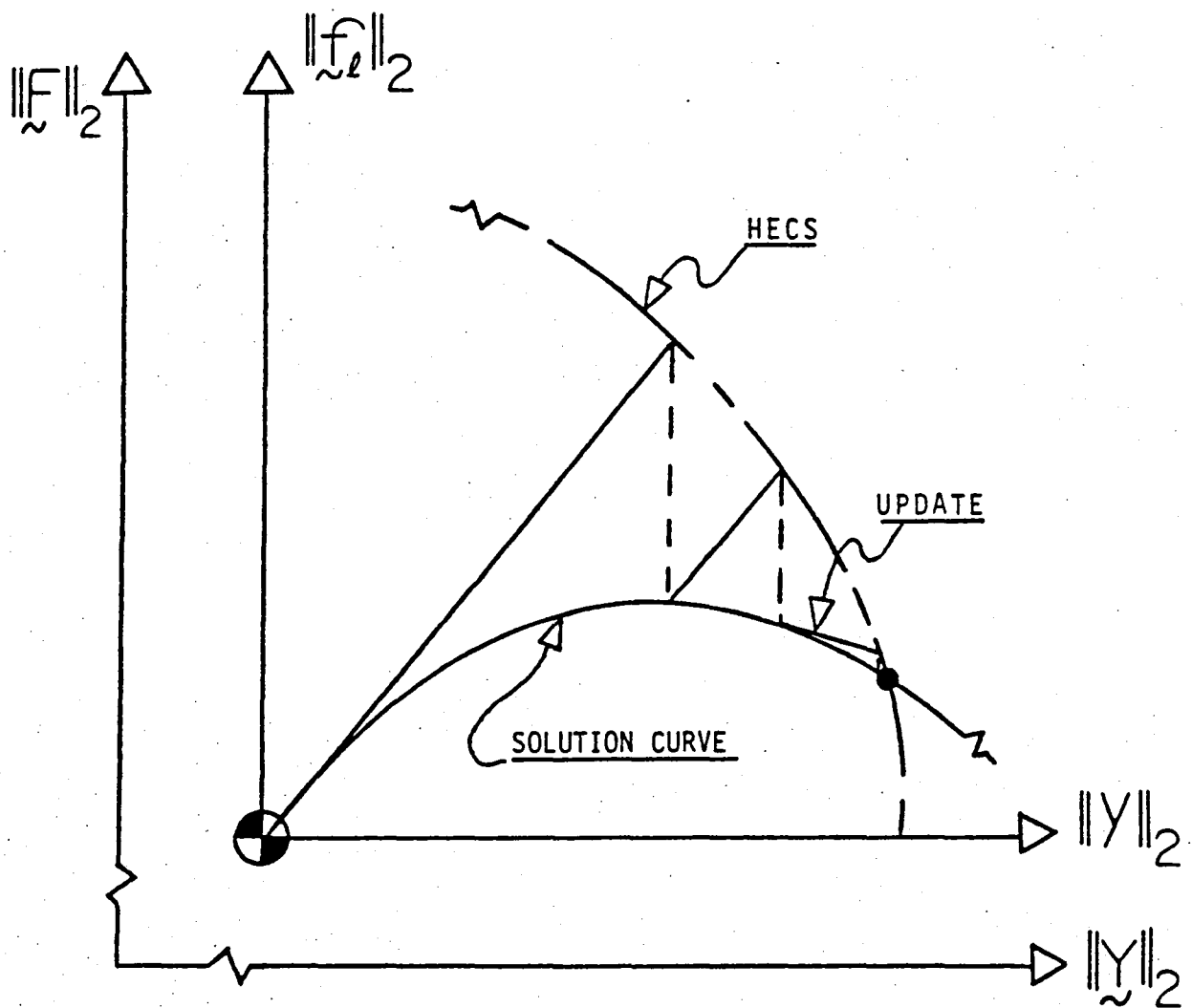


FIG.6 Iterative process associated with turning point without updating

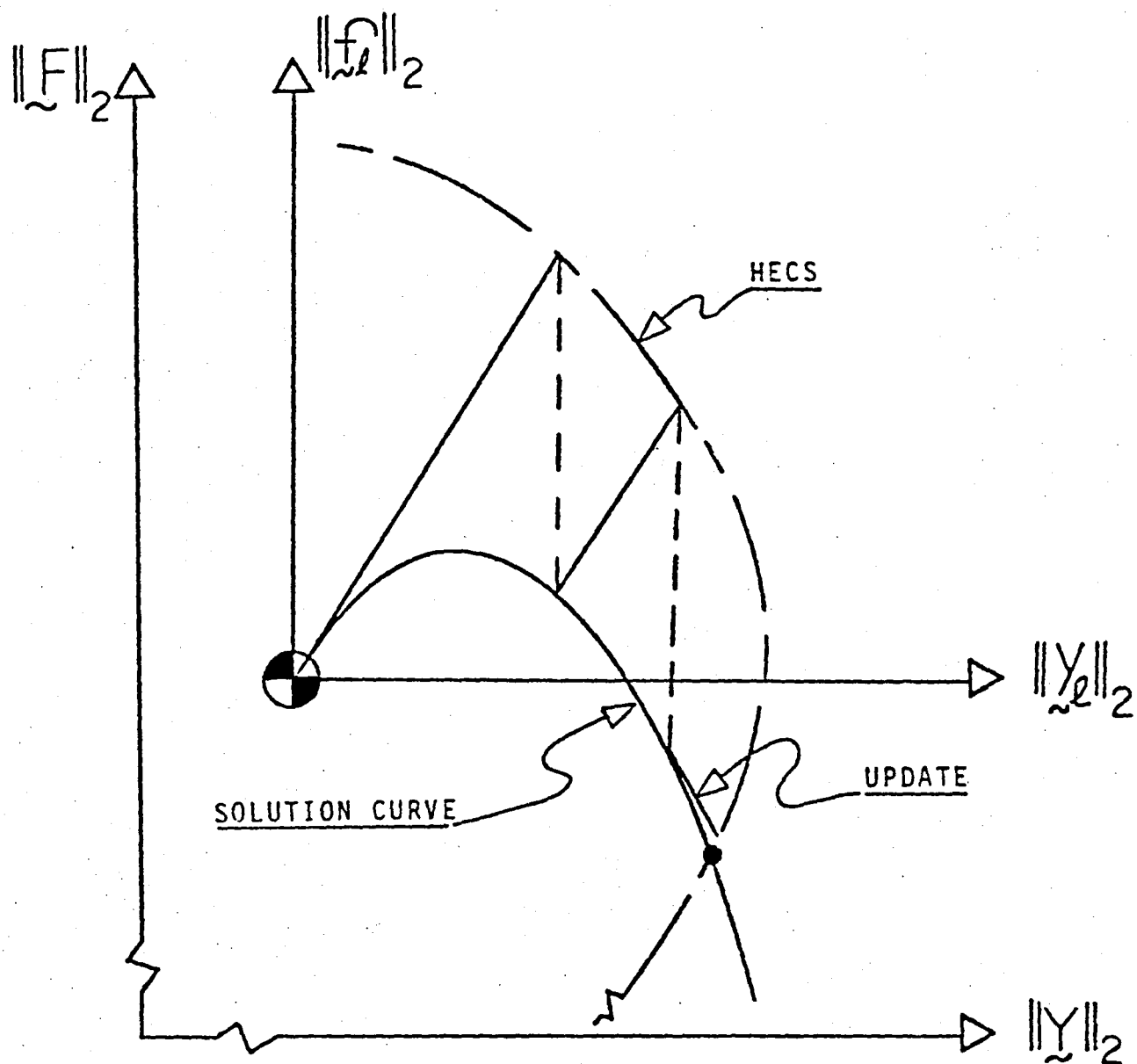


FIG. 7 Iterative process associated with turning point with updating

Similar results can also be ascertained by monitoring the "above/belowness" relative to the  $||\underline{y}||_2$  axis of the HECS, namely

$$||\underline{F}(\underline{y}_\ell^0)||_2 \begin{cases} > ||\underline{F}(\underline{y}_\ell^{i-1})||_2; \text{ below} \\ < ||\underline{F}(\underline{y}_\ell^{i-1})||_2; \text{ above} \end{cases} \quad (3.34)$$

Adjusting for the initial curvature of the given load increment, the following condition flag can be used to establish the requisite restructuring of the  $\lambda_\ell^i$  algorithm, that is

$$\phi_\ell^{i-1} = \text{sgn} ( ||\underline{F}(\underline{y}_\ell^{i-1})||_2 - ||\underline{F}(\underline{y}_\ell^0)||_2 ) \quad i > 1 \quad (3.35)$$

where sign changes signal the need for stiffness updating such that

$$\phi_\ell^{i-1} = \begin{cases} -1; \text{ below origin} \\ +1; \text{ above origin} \end{cases} \quad (3.36)$$

In terms of (3.35), the CMINR algorithm takes the following form:

$$\lambda_\ell^i = \frac{1}{2\Xi_{\ell 1}^{i-1}} \{ -\Xi_{\ell 2}^{i-1} + \phi_\ell^{i-1} [(\Xi_{\ell 2}^{i-1})^2 - 4\Xi_{\ell 2}^{i-1} \Xi_{\ell 3}^{i-1}]^{1/2} \} \quad (3.37)$$

Note, to keep the above noted algorithmic flow consistent, the  $\pm$  signs appearing in (3.27) must be replaced by  $\text{sgn}(C_R^\ell)$ . This will yield the proper succession of  $\underline{F}$ .

### 3.2 Adaptive Warp of HECS

To establish  $\mu_\ell$ , the local curvature of the force displacement space is required. In this context, the curvature parameter of Bergan et al. [9] is particularly useful as it represents a measure of the local definiteness (positive or indefinite). For the present purposes, to establish such a relation, assuming that

$\Delta \tilde{F}_\ell$  is a constant, then  $\tilde{F}_\ell$  is defined by the single parameter relation

$$\tilde{F}_\ell = \Lambda_\ell \Delta \tilde{F} \quad (3.38)$$

where

$$\Lambda_\ell = \sum_{k=1}^{\ell} \lambda_k^I \quad (3.39)$$

In terms of (3.39), the curvature parameter is obtained by taking the ratio of the inner products of  $\Delta \tilde{F}$  and the derivative of the nodal displacement via  $\Lambda_k$  evaluated at  $k=1$  and  $\ell-1$  respectively. This yields the expansion

$$C_R^\ell = (\Delta \tilde{F})^T \frac{d}{d\Lambda} (\tilde{Y}) |_{\Lambda_{\ell-1}} / ((\Delta \tilde{F})^T \frac{d}{d\Lambda} (\tilde{Y}) |_{\Lambda_1}) \quad (3.40)$$

where employing backward finite differences [23], the foregoing derivatives can be approximated by

$$\frac{d}{d\Lambda} (\tilde{Y}) |_{\Lambda_{\ell-1}} \sim \frac{1}{\lambda_{\ell-1}^I} \tilde{Y}_{\ell-1} + O((\lambda_{\ell-1}^I)^2) \quad (3.41)$$

In terms of (3.41), (3.40) reduces to

$$C_R^\ell \sim (\Delta \tilde{F})^T \Delta \tilde{Y}_{\ell-1} \lambda_1^I / ((\Delta \tilde{F})^T \Delta \tilde{Y}_1 \lambda_{\ell-1}^I) \quad (3.42)$$

such that  $\Delta \tilde{Y}_1$  and  $\Delta \tilde{Y}_{\ell-1}$  represent the total variations in nodal displacements associated with the first and  $(\ell-1)^{th}$  load increments.

The curvature parameter can be further modified by noting that for small enough excursions, it follows that

$$\lambda_k^I \Delta \tilde{F} \sim [K_T(\tilde{Y}_{k-1})] \Delta \tilde{Y}_k \quad (3.43)$$

hence

$$C_R^\ell = \frac{(\Delta \tilde{Y}_{\ell-1})^T [K_T(\tilde{Y}_\ell^0)] \Delta \tilde{Y}_{\ell-1}}{(\Delta \tilde{Y}_1)^T [K_T(\tilde{Y}_2^0)] \Delta \tilde{Y}_1} \left( \frac{\lambda_1^I}{\lambda_{\ell-1}^I} \right)^2 \quad (3.44)$$

where here, the denominator is a direct measure of the incremental energy stored during the first load step while the numerator denotes the second variation of energy associated with the  $(\ell-1)^{th}$  load increment.

The parameter  $C_R^\ell$  can be used to scale  $\mu_\ell$ . To start this development, it follows that during the initial stages of any loading process, only modest changes typically occur in  $[K_T]$  hence few iterations occur during say the first increment. Thus

$$\Delta \tilde{Y}_1 \sim [K_T(0)]^{-1} \Delta \tilde{F} \quad (3.45)$$

or in a normed sense

$$||\Delta \tilde{Y}_1||_2 \leq ||[K_T(0)]^{-1} \Delta \tilde{F}||_2 \quad (3.46)$$

Recalling the HECS, it follows that the upper bound value of  $\Delta \tilde{Y}_1$  is given by

$$\lim_{f \rightarrow 0} ||\Delta \tilde{Y}_1||_2 \leq \frac{1}{\mu_\ell} ||\Delta \tilde{F}||_2 \quad (3.47)$$

and hence,

$$\Delta \tilde{Y}_1 \leq \frac{1}{\sqrt{\mu_\ell}} \Delta \tilde{F} \quad (3.48)$$

Comparing (3.46) and (3.47), it follows that a good initial value of  $\mu_\ell$  can be taken as

$$\mu_1 (\text{initial}) = \frac{N_S}{\alpha} \quad (3.49)$$



where

$$N_s = ||\Delta \tilde{F}||_2 / ||[K_T(\tilde{Q})]^{-1} \Delta \tilde{F}||_2 \quad (3.50)$$

such that  $\alpha$  is a user selected parameter which enables an expansion or contraction capability for the HECS. Now as we proceed to successive load steps,  $\mu_\ell$  must be scaled to reflect potential curvature changes in the force-deflection space. Since  $C_R^1 = 1$ , this can be achieved by letting

$$\mu_\ell = \frac{N_s}{\alpha (C_R^\ell)^\beta} \quad (3.51)$$

where  $\beta$  enables the user to vary the influence of the curvature parameter in defining the warping of the HECS.

#### 4. ENERGY CONSTRAINT: CORRECTOR PHASE

As noted earlier, for the present purposes the CMINR is employed in the manner of a predictor algorithm. To correct the results arising from this stage of calculation, a strain energy constraint will be employed to enforce the proper type of monotonicity of successive solution iterates. This is achieved by upper bounding the admissible strain energy excursion by scaling the variation of load and deflection during the iteration process. Such scaling can either be based on worst case individual element constraint tests or on an overall global check. If the check is failed, to provide for the foregoing scaling, the HECS is shrunk so as to maintain the requisite convergence characteristics.

To initiate the development, a workable expression must be obtained for successive strain energy excursions generated during the iterative process. In this context, a trapezoidal approximation

is employed to evaluate the incremental area "under" the solution curve. Specifically the energy accumulated during the  $i^{\text{th}}$  iteration of the  $\ell^{\text{th}}$  load increment takes the following form namely

$$\Delta E_{\ell}^i = \frac{1}{2} (\Delta \tilde{Y}_{\ell}^i)^T (\tilde{F}(\tilde{Y}_{\ell}^i) + \tilde{F}(\tilde{Y}_{\ell}^{i-1})) + O((\|\Delta \tilde{Y}_{\ell}^i\|_2)^2) \quad (4.1)$$

where

$$\tilde{F}(\tilde{Y}_{\ell}^{i-1}) = \int_R [B^*(\tilde{Y}_{\ell}^{i-1})]^T \tilde{S}(\tilde{Y}_{\ell}^{i-1}) dv \quad (4.2)$$

$$\tilde{F}(\tilde{Y}_{\ell}^i) = \int_R [B^*(\tilde{Y}_{\ell}^i)]^T \tilde{S}(\tilde{Y}_{\ell}^i) dv \quad (4.3)$$

To achieve the requisite scaling of the governing field variables,  $\tilde{Y}_{\ell}^i$  is recast as follows

$$\tilde{Y}_{\ell}^i = \tilde{Y}_{\ell}^{i-1} + \chi_{\ell}^i \Delta \tilde{Y}_{\ell}^i \quad (4.4)$$

where the scaling parameter  $\chi_{\ell}^i$  must be chosen to enforce the following energy constraint namely

$$\Delta E_{\ell}^i < e_R \Delta E_{\ell}^{i-1}; \quad i = 2, 3, \dots \quad (4.5)$$

such that  $e_R$  is a user selected parameter which can either loosen or tighten the monotonicity requirements. Hence, once  $e_R$  is selected, (4.1) and (4.5) lead to the requisite value of  $\chi_{\ell}^i$ . In terms of  $\chi_{\ell}^i$ , the HECS can be warped in the abscissa dimension by letting  $\mu_{\ell} \rightarrow \mu_{\ell}/\chi_{\ell}^i$ . This effectively reduces its size thereby providing a tighter bound on successive  $\Delta \tilde{Y}_{\ell}^i$ .

To obtain the foregoing scaling,  $\chi_{\ell}^i$  must be extracted from (4.1) and (4.5). In this context, since  $\tilde{F}(\tilde{Y}_{\ell}^i)$  is dependent on the disposition of the energy constraint/scaling parameter  $\chi_{\ell}^i$ , in terms of (4.4), (4.3) can be recast as follows namely

$$\begin{aligned}
F(\tilde{y}_\ell^i) = & F(\tilde{y}_\ell^{i-1}) + x_\ell^i \int_R [K_T(\tilde{y}_\ell^{i-1})] dv \Delta y_\ell^i + \\
& (x_\ell^i)^2 \int_R ([G]^T [B_n(\Delta y_\ell^i)]^T [D_T] [B^*(\tilde{y}_\ell^{i-1})] + \\
& [B^*(\tilde{y}_\ell^{i-1})]^T [D_T] [B_n(\Delta y_\ell^i)] [G]) dv \Delta y_\ell^i + \\
& (x_\ell^i)^3 \int_R [G]^T [B_n(\Delta y_\ell^i)]^T [D_T] [B_n(\Delta y_\ell^i)] [G] dv \Delta y_\ell^i
\end{aligned} \tag{4.6}$$

or in approximate form by

$$F(\tilde{y}_\ell^i) = F(\tilde{y}_\ell^{i-1}) + x_\ell^i \int_R [K_T(\tilde{y}_\ell^{i-1})] dv \Delta y_\ell^i + O((x_\ell^i)^2) \tag{4.7}$$

Employing (4.6), the energy stored during the  $i$ th iteration can be written in the form

$$\begin{aligned}
\Delta E_\ell^i = & \frac{1}{2} x_\ell^i \Delta y_\ell^i \{ 2F_\ell^{i-1} + x_\ell^i \int_R [K_T(\tilde{y}_\ell^{i-1})] dv \Delta y_\ell^i + \\
& (x_\ell^i)^2 \int_R ([G]^T [B_n(\Delta y_\ell^i)]^T [D_T] [B^*(\tilde{y}_\ell^{i-1})] + \\
& [B^*(\tilde{y}_\ell^{i-1})]^T [D_T] [B_n(\Delta y_\ell^i)] [G]) dv \Delta y_\ell^i + \\
& (x_\ell^i)^3 \int_R [G]^T [B_n(\Delta y_\ell^i)]^T [D_T] [B_n(\Delta y_\ell^i)] [G] dv \Delta y_\ell^i
\end{aligned} \tag{4.8}$$

Rearranging (4.8), we have that

$$\Delta E_\ell^i = x_\ell^i \Gamma_{\ell 1}^i + (x_\ell^i)^2 \Gamma_{\ell 2}^i + (x_\ell^i)^3 \Gamma_{\ell 3}^i + (x_\ell^i)^4 \Gamma_{\ell 4}^i \tag{4.9}$$

where the various bilinear coefficients take the form

$$\Gamma_{\ell 1}^i = (\Delta Y_{\ell}^i)^T E_{\ell}^{i-1} \quad (4.10)$$

$$\Gamma_{\ell 2}^i = \frac{1}{2} (\Delta Y_{\ell}^i)^T [K_T(Y_{\ell}^{i-1})] \Delta Y_{\ell}^i \quad (4.11)$$

$$\Gamma_{\ell 3}^i = \frac{1}{2} (\Delta Y_{\ell}^i)^T \int_R ([G]^T [B_n (\Delta Y_{\ell}^i)^T [D_T] [B^*(Y_{\ell}^{i-1})]] + [B^*(Y_{\ell}^{i-1})]^T [D_T] [B_n (\Delta Y_{\ell}^i)] [G]) dv \Delta Y_{\ell}^i \quad (4.12)$$

$$\Gamma_{\ell 4}^i = \frac{1}{2} \Delta Y_{\ell}^i \int_R [G]^T [B_n (\Delta Y_{\ell}^i)]^T [D_T] [B_n (\Delta Y_{\ell}^i)] [G] dv \Delta Y_{\ell}^i \quad (4.13)$$

Truncating (4.8) to  $O((x_{\ell}^i)^2)$  or less yields the following more tractable algorithmic expression for  $\Delta E_{\ell}^i$ , that is

$$\Delta E_{\ell}^i \sim x_{\ell}^i \Gamma_{\ell 1}^i + (x_{\ell}^i)^2 \Gamma_{\ell 2}^i + O((x_{\ell}^i)^2) \quad (4.14)$$

Now, enforcing the energy constraint defined by (4.5), the following general and reduced polynomial expressions are obtained for  $x_{\ell}^i$ , that is

$$(x_{\ell}^i)^4 \Gamma_{\ell 4}^i + (x_{\ell}^i)^3 \Gamma_{\ell 3}^i + (x_{\ell}^i)^2 \Gamma_{\ell 2}^i + (x_{\ell}^i) \Gamma_{\ell 1}^i - e_R E_{\ell}^{i-1} \leq 0 \quad (4.15)$$

or more simply

$$(x_{\ell}^i)^2 \Gamma_{\ell 2}^i + x_{\ell}^i \Gamma_{\ell 1}^i - e_R E_{\ell}^{i-1} \leq 0 \quad (4.16)$$

For simplicity, solving (4.16) for  $x_{\ell}^i$  yields

$$x_{\ell}^i = \frac{1}{2\Gamma_{\ell 2}^i} \left\{ -\Gamma_{\ell 1}^i + [(\Gamma_{\ell 1}^i)^2 + 4e_R E_{\ell}^{i-1} \Gamma_{\ell 2}^i]^{\frac{1}{2}} \right\} \quad (4.17)$$

where for PD situations  $\Gamma_{\ell 2}^i > 0$ . As noted earlier,  $\chi_{\ell}^i$  defined by (4.17) can be used to resize the HECS thereby providing for a tighter bound on successive iterations. Having now obtained the proper scaling, the energy stored during the  $\ell^{\text{th}}$  load increment is given by

$$E_{\ell \text{tot}} = \sum_{i=1}^I \Delta E_{\ell}^i \quad (4.18)$$

where here  $\Delta E_{\ell}^i$  is defined by (4.9) such that local MDPD solution curvature is assumed. In such situations, it follows that

$$\Delta E_{\ell}^i > 0 \text{ for } \forall i \quad (4.19)$$

Similar monotone behavior of the energy increments is also noted for MIID solution curvature.

In the case of MIPD and MDID curvatures, since successive iterates form an oscillatory nonmonotone sequence, the energy increments themselves give rise to an alternating sequence of positive and negative definite terms. For such a situation, the specific definiteness of successive energy increments is defined as follows:

$$\Delta E_{\ell}^i \begin{cases} > 0 \text{ if } \phi_{\ell}^{i-1} < 0, \phi_{\ell}^i > 0 \\ < 0 \text{ if } \phi_{\ell}^{i-1} > 0, \phi_{\ell}^i < 0 \end{cases} \quad (4.20)$$

## 5. SUMMARY AND DISCUSSION OF NUMERICAL EXPERIMENTS

The overall algorithmic flow associated with the predictor-corrector procedure is performed in several main steps. These include:

- i) The monitoring of the various condition flags;

- ii) The application of the various predictor-corrector constraint algorithms; and lastly,
- iii) The assessment of convergence.

For the purposes of algorithmic efficiency, the various condition flags can themselves be applied in three main levels which have the following purposes namely:

- i) To define the geometry of the HECS contingent upon local solution curvature; calculate  $C_R^\ell$ ,  $\mu_\ell$ ;
- ii) Locate solution positioning relative to HECS so as to enable proper structuring of algorithms; calculate  $\Xi_\ell^{i-1}$ ,  $\phi_\ell^{i-1}$ ,  $K_\mu^{\ell i}$  and;
- iii) Define conditioning of iterated solution curve via several flags noting need for updating and constraint tightening; calculate  $\chi_\ell^i$  etc.

As noted earlier, depending on the various condition flags, iteration count and user options, the stiffness may be updated and inverted in the following manner:

- i) Preferential local updates of highly nonlinear elements [14];
- ii) Standard full global update;
- iii) Pseudo updates (BFGS [18], Broyden [24], DFP [25], Huang [26], etc.);
- iv) Update only at start of given load increment loop.

Such actions are preparatory to the application of the various predictor/corrector algorithms. The predictor phase consists of

projecting the solution curve via the MINR, INR or pseudo INR algorithms to determine its intersection with the HECS. The corrector phase employs an energy constraint to enforce the proper type of convergence. This is achieved by upper bounding the admissible energy excursion by scaling the variation of load and deflection during the iteration process. Such scaling can either be based on worst case individual element constraint tests or an overall global check. For the present purposes, the three phases of convergence testing discussed by Padovan [14] are advocated here. There consist of:

- i) Displacement/force norm checks;
- ii) Quality of convergence tests; and,
- iii) Nonlinearity checks.

As a demonstration of the approach developed herein, we consider the following highly nonlinear numerical experiments, namely:

- i) Stretching of a rubber sheet;
- ii) Large deformation loading of a spherical cap; and,
- iii) Pre- and postbuckling of a centrally loaded arch.

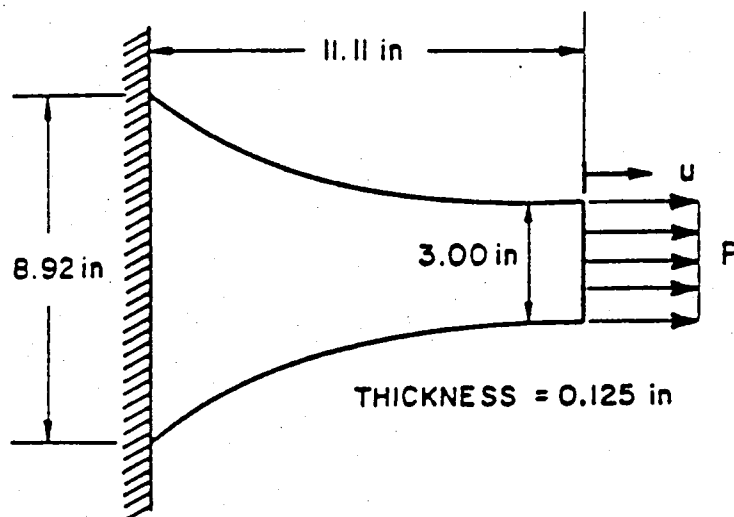
These problems were chosen to illustrate the predictor-correctors capability and efficiency to handle varying types of kinetic, kinematic and material induced nonlinearity. To enable the calculations, special predictor-corrector "plug ins" were developed for the ADINA code of Bathe [27].

To start, the stretching of a rubber sheet is treated first. This problem involves both large deformation kinematics and kinetics as well as significant material nonlinearity of the Mooney-Rivlin

type [28]. Figure (8) illustrates the geometry, material properties as well as the FE mesh used to simulate the problem. Based on the use of 2-D plane stress 8 node isoparametric elements, Figures (9 and 10) show various aspects of the response behavior of the rubber sheet to wide ranging loads. In addition, Figure (9) also lists a comparison of the required number of iterations for the MINR and predictor-corrector algorithms over the same load range. As can be seen, for the given problems, the current approach is more efficient. In particular as seen from Figure 9 a 40% improvement is achieved for the given problem. This follows from the fact that the HECS tends to generate a larger driving force potential over the classic INR for the same size load step. Because of this, fewer iterations are required. More importantly is the fact that the entire iteration process is automatic. The only data needed is the final load step. Once specified, the load stepping becomes self-adaptive. Note, while  $\alpha$ ,  $\beta$  and  $e_p$  are user selectable, for all the problems considered herein, unity values proved to yield satisfactory results.

Note while the rate of convergence can be modified by changing the various conditioning parameters, due to the constraining nature of the predictor-corrector algorithm, "unbounded" iterate excursions are precluded from occurring. Because of this, unlike the INR algorithm which yields strongly divergent and unstable successive iterates when excessive load steps are employed, the current approach tends to yield a stable solution even when a relatively large HECS and loose energy constraint are employed. Whatever solution drift that might occur is entirely removed by only moderate tightening of the constraints. This strongly stable characteristic makes the predictor-corrector algorithm more forgiving as to conditioning choices.



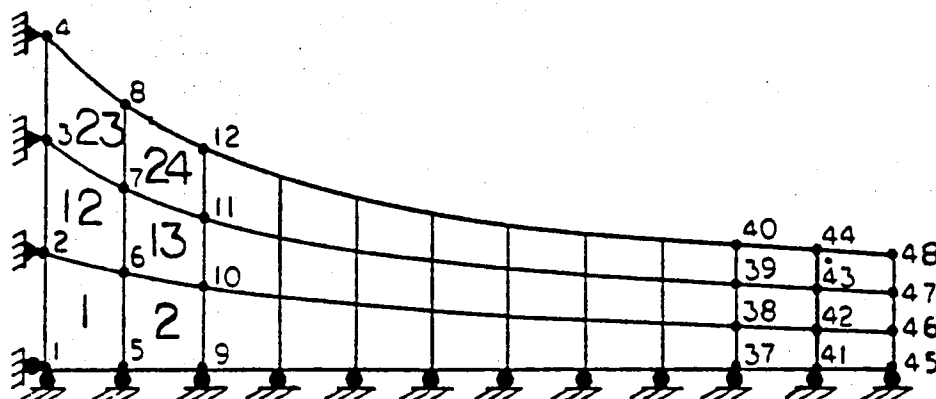


RUBBER SHEET

MATERIAL PROPERTIES

$$C_1 = 21.605 \text{ lb/in}^2$$

$$C_2 = 15.747 \text{ lb/in}^2$$



FINITE ELEMENT MESH ( 4 NODE ELEMENTS)

FIG.8 FE simulation of rubber sheet

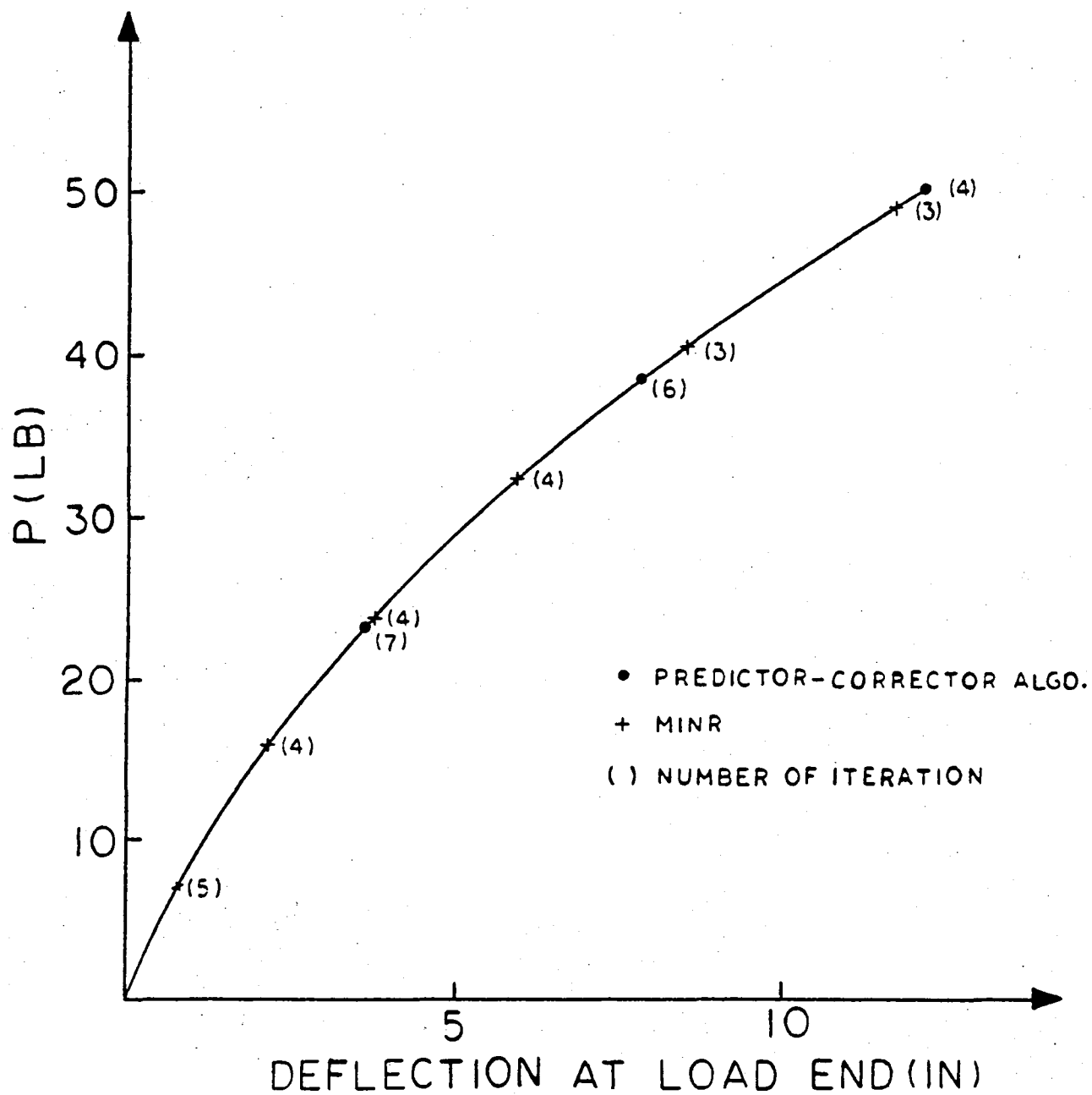


FIG.9 Load deflection curve of rubber sheet

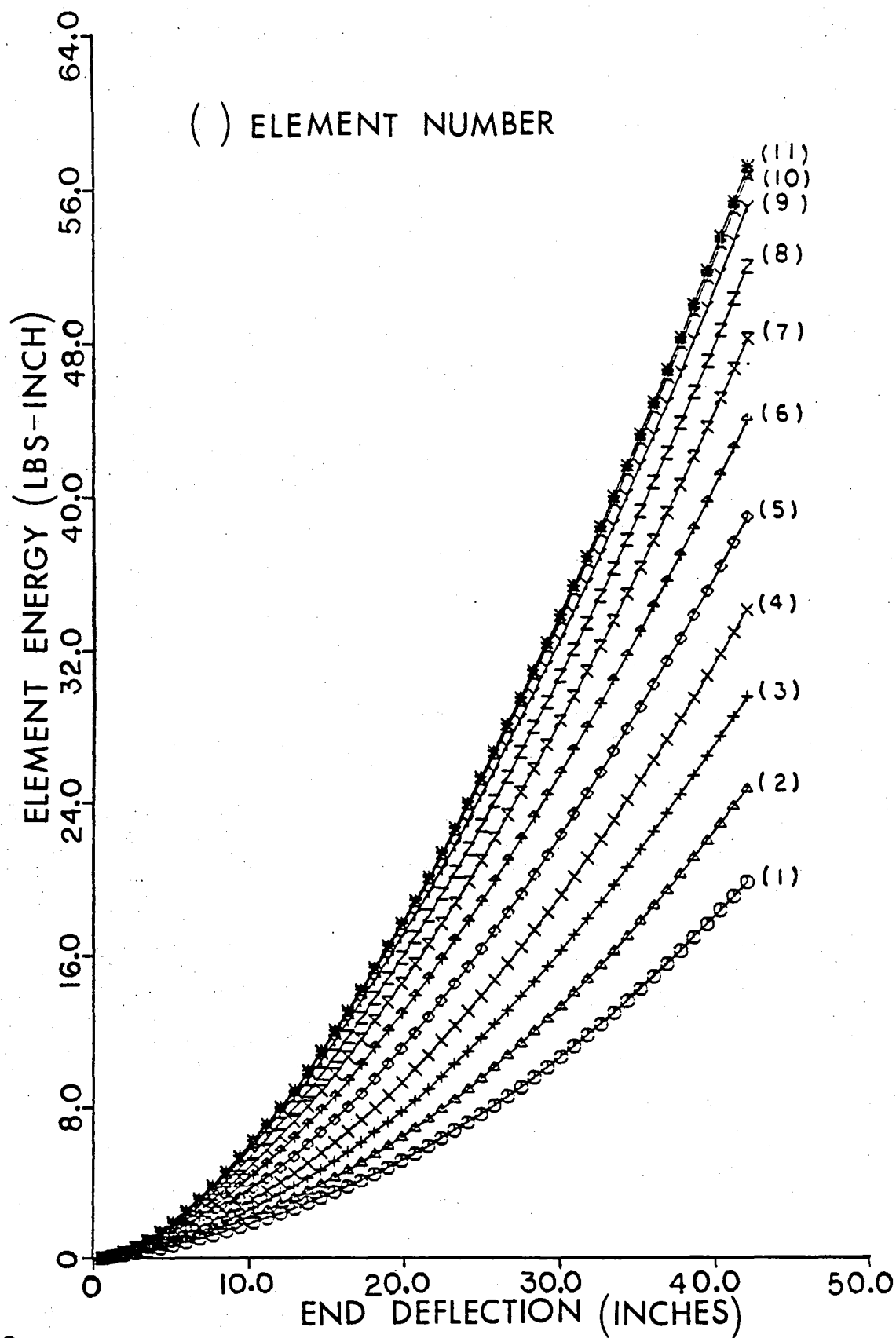


FIG. 10 Strain energy space of rubber sheet

In terms of the spherical cap problem defined in Fig. 11, Fig. 12 clearly demonstrates the foregoing behavioral characteristics. In particular, as the HECS is tightened, the correct limiting behavior is obtained. Note the other results [27] juxtaposed on this Figure were obtained through the use of the INR wherein iteration was suspended and hence represents essentially a straight Euler-Cauchy type incrementation without regard to unbalance loads. When iteration is readmitted into the calculations, the INR yields highly unstable and divergent solution behavior. This is a direct outgrowth of the fact that for the given cap geometry, while the global load deflection characteristics show positive definite behavior, significant unloading occurs locally. As seen in Fig. (13), the slopes of the local element energy-load parameter space undergo fluctuations in definiteness. Because of this, the overall stiffness can exhibit local "shallowness" hence leading to anomalous excursions of the nodal displacements of a given element. For the classic INR type operator, such local overshoot tends to grow in magnitude as well as spread to neighboring elements ultimately leading to a globally divergent solution. For the current approach such behavior is completely eliminated by the use of the HECS and energy constraint. Because of this, successive iterations can be used to eliminate any load imbalances and hence drift.

Note, for the results depicted in Figure 12, the CINR generated results were between 70-80% faster than the standard INR with iteration suspended. If small amounts of drift were allowed in the CINR, 5% max, the speed of calculation improved to the range 140-100%

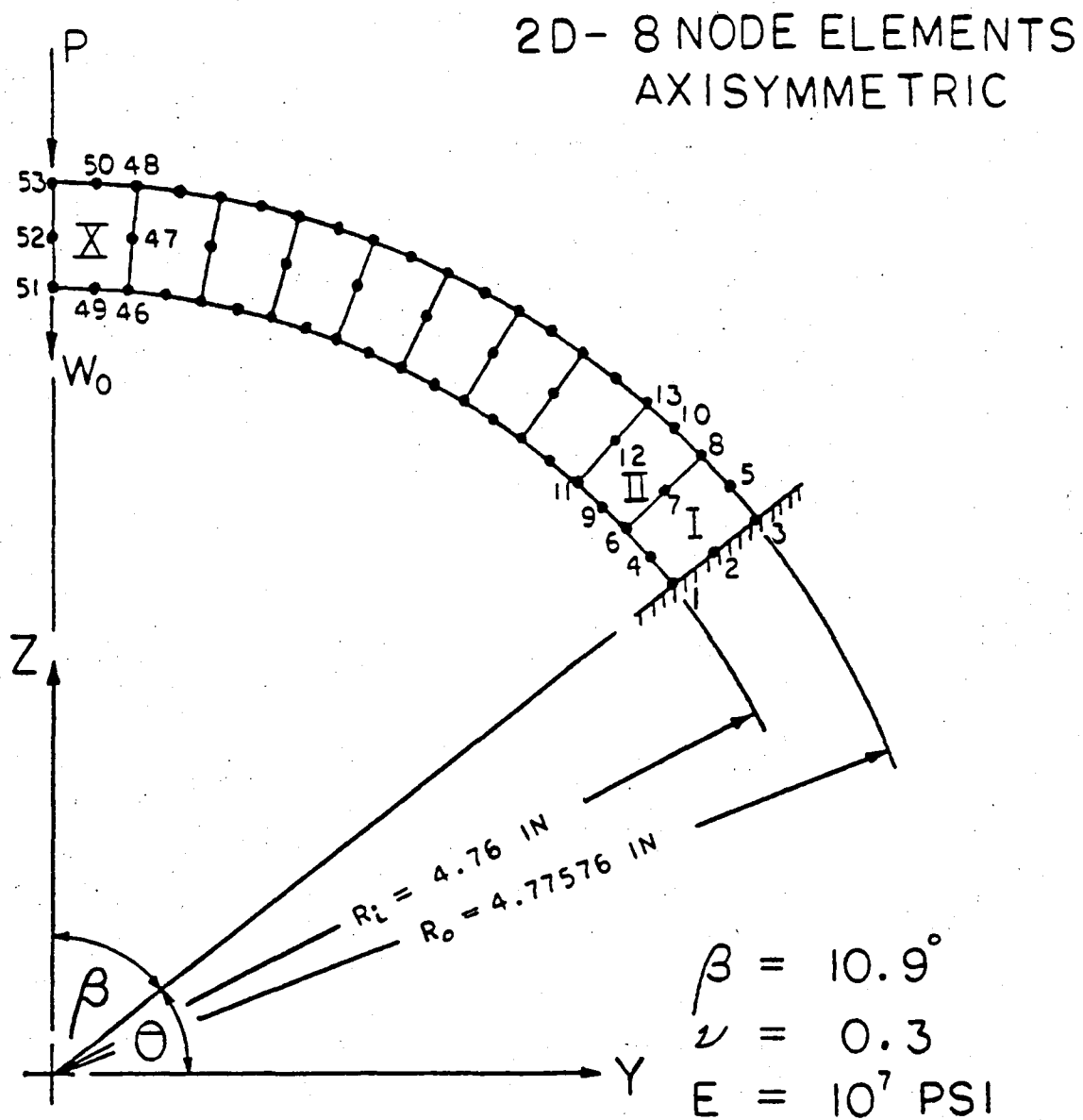


FIG. 11 FE simulation of spherical cap

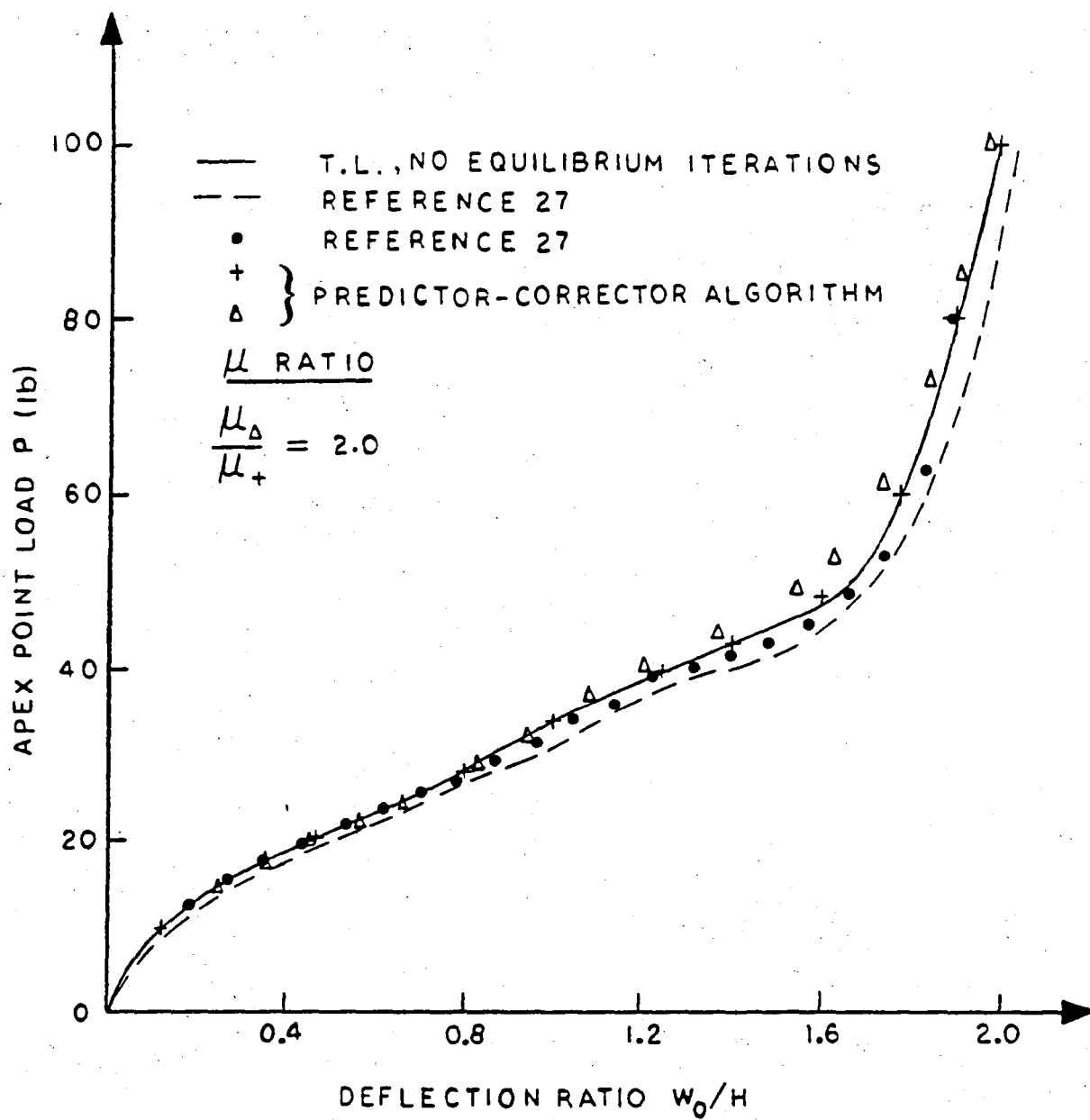


FIG. 12 Load deflection curve of spherical cap

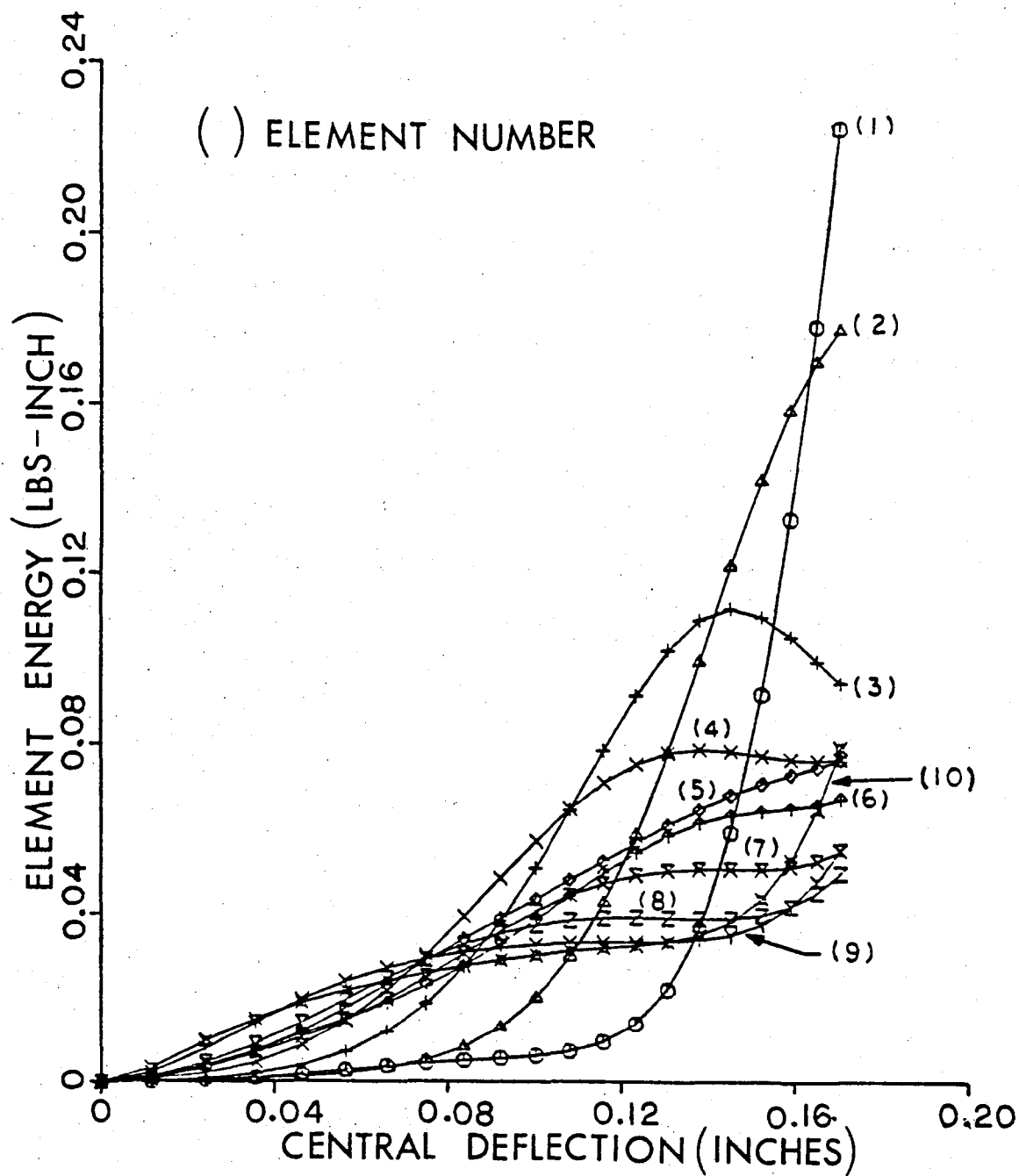


FIG.13 Strain energy space of spherical cap

times faster. If the same was attempted for the INR, as noted above, divergent solution behavior was immediately encountered. The foregoing speed enhancements are associated with the form of nonlinearity treated. Had other types been considered, the speed enhancements would have varied depending on the generic curvature changes encountered.

Figure (14) illustrates the geometry and finite element model of a centrally loaded shallow arch. The model employs plane stress eight node isoparametric elements. As seen from Figure (15), good correlation is obtained with previous analytical [29] and experimental [30] results. The local load/unload characteristics of the pre- to postbuckling transitions are clearly seen in Figure (16). As with the cap problem, local changes in definiteness occur in the energy-load parameter space. For the given arch though, such definiteness fluctuations are significant enough to lead to unloading/reloading in the postbuckling zone.

## 6. CONCLUSIONS

In terms of the foregoing numerical experiments, it follows that the predictor-corrector algorithm can handle essentially all the types of nonlinearities prevalent to the nonlinear responses of structures in a highly efficient and self-adaptive fashion. This includes situations which undergo definiteness changes as in turning points and bifurcations. Because of the manner of the formulation, the procedure is applicable to history dependent situations involving creep and plasticity. Lastly, due to the form



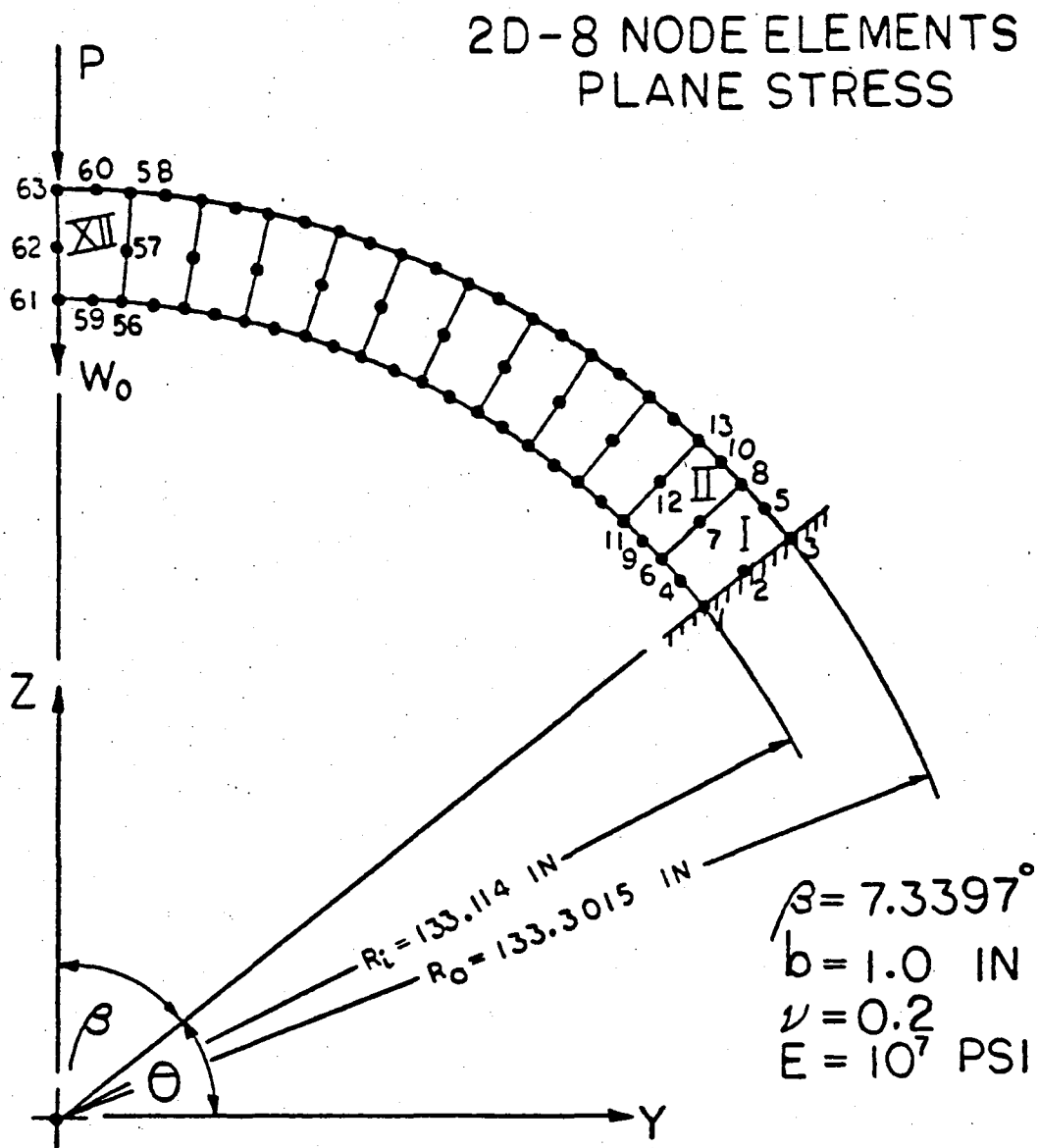


FIG. 14 FE simulation of arch

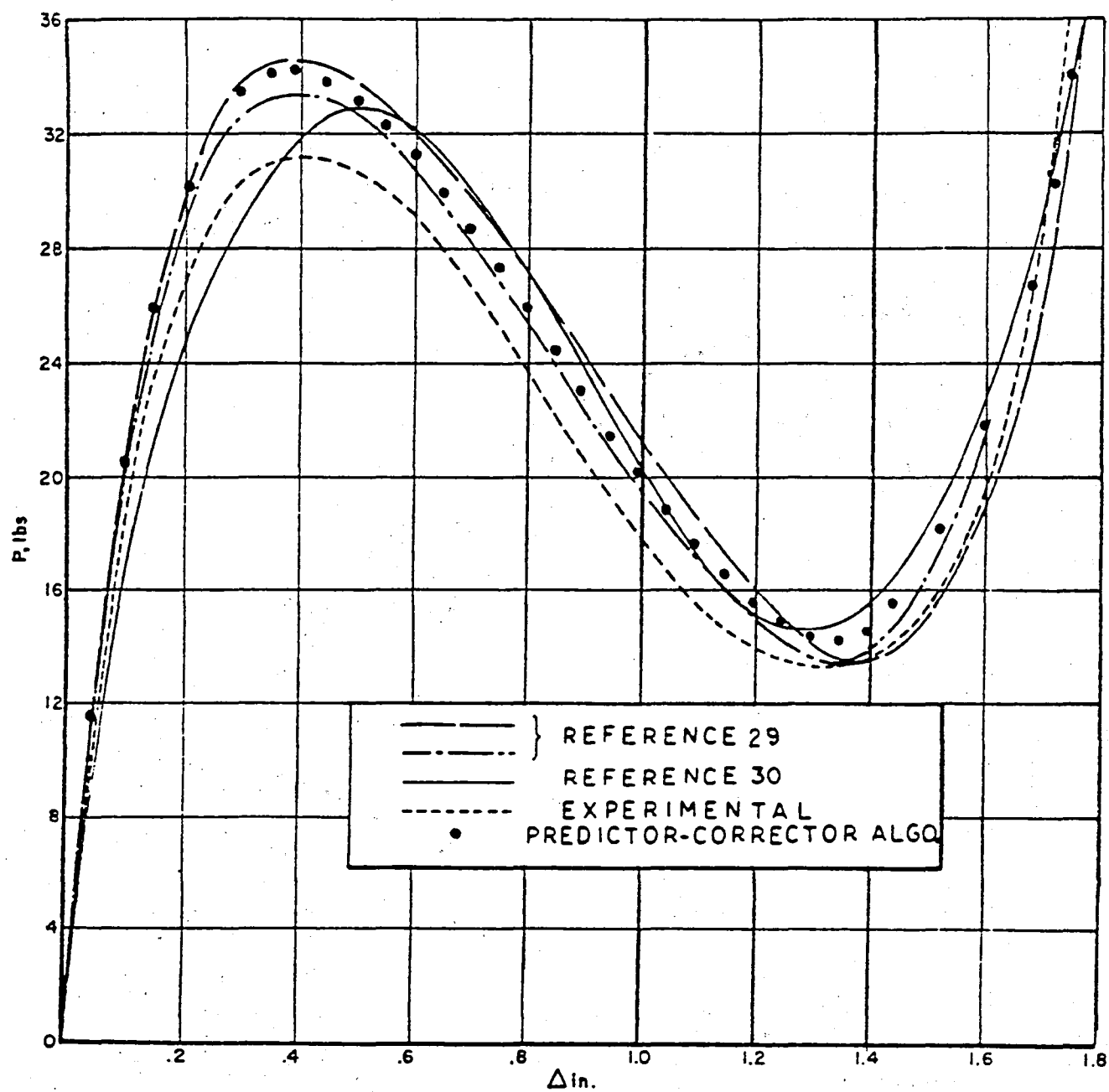


FIG.15 Load deflection curve of arch

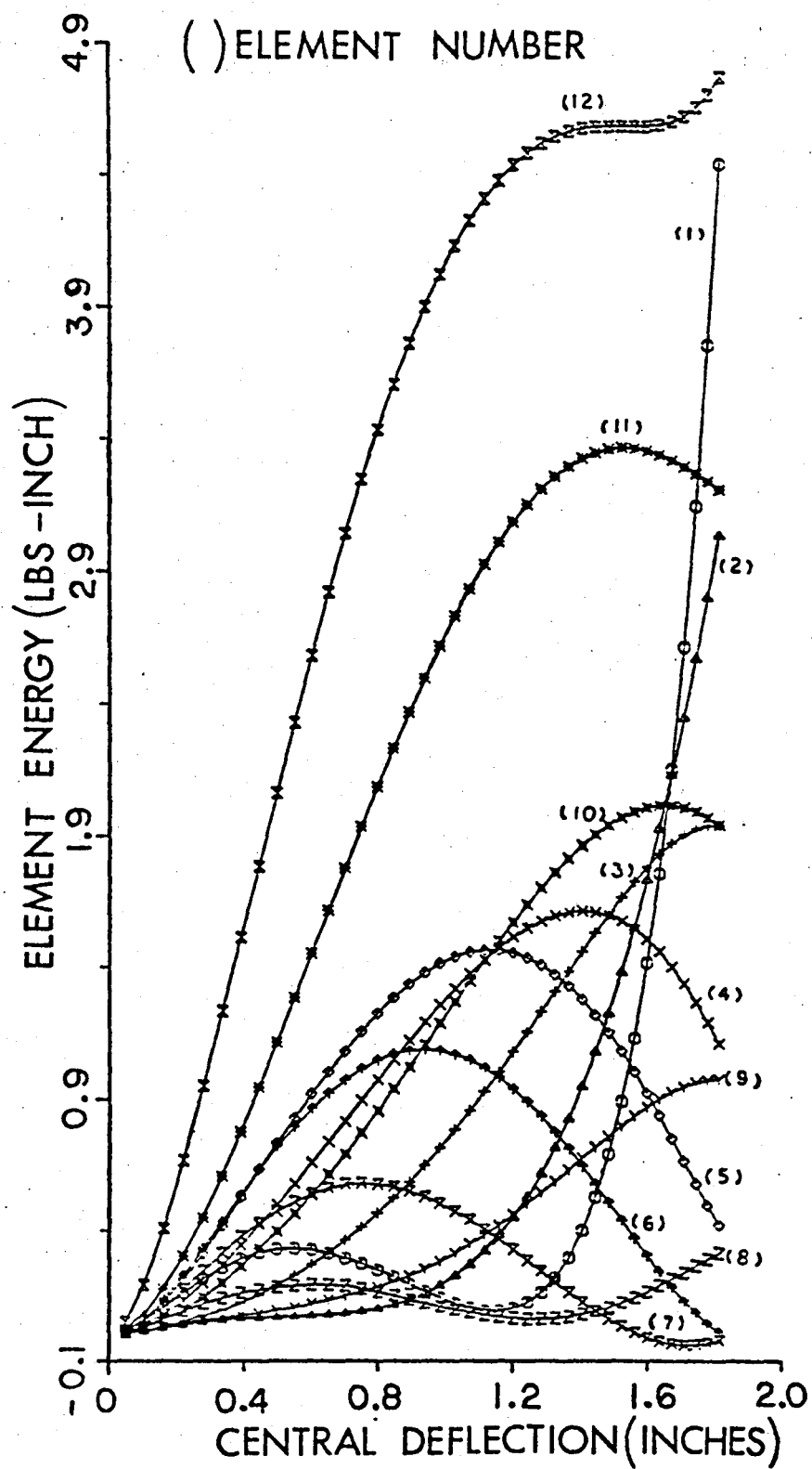


FIG. 16 Strain energy space of arch

of its algorithmic "hardware", it can be easily implanted into currently available GP nonlinear codes without any need for major architectural modification.

#### Acknowledgement

The author is grateful to Dr. C. Chamis of NASA-Lewis for the stimulating discussions and encouragements during the course of this work.

## References

1. J. T. Oden, "Finite Elements of Nonlinear Continua", McGraw-Hill, New York, 1972.
2. J. A. Stricklin, W. E. Haisler and W. A. von Rieseemann, "Evaluation of Solution Procedures for Material and/or Geometrically Nonlinear Structural Analysis", AIAA J. 11, 292-299 (1973).
3. J. R. Tillerson, J. A. Stricklin and W. E. Haisler, "Numerical Methods for the Solution of Nonlinear Problems in Structural Analysis", ASME Winter Annual Meeting, Detroit, November (1973), in Numerical Solution of Nonlinear Structural Problems (Ed. R. F. Hartung), AMD, Vol. 6, 1973, pp. 67-101.
4. P. G. Bergan and T. H. Soreide, "A Comparative Study of Different Solution Techniques as Applied to a Nonlinear Structural Problem", Computer Meth. Appl. Mech. Engrg. 2, 185-201 (1973).
5. R. H. Gallagher, "Finite Element Analysis of Geometrically Nonlinear Problems in Theory and Practice in Finite Element Structural Analysis" (Ed. Y. Yamada and R. H. Gallagher), University of Tokyo Press, 1973, pp. 109-123.
6. R. H. Gallagher, "Element and Global Formulations and Solution Algorithms for Geometrically Nonlinear Analysis", ICCAD Course Advanced Topics in Finite Element Analysis, Santa Margherita, Italy (1974), Lecture Series No. 1/74, Chapter 12.
7. C. A. Felippa, "Procedures for Computer Analysis of Large Nonlinear Structural Systems", Int. Symp. Large Engrg. Systems, Winnipeg (1976), published in Large Engineering Systems (Ed. A. Wexler), Pergamon, Oxford, (1977).
8. W. Haisler, J. Stricklin and J. Key, "Displacement Incrementation in Non-linear Structural Analysis by the Self-Correcting Methods", Int. J. num. Meth. Engrg. 3-10 (1977).
9. P. G. Bergan, G. Horrigmoe, B. Krakeland and T. H. Soreide, "Solution Techniques for Non-linear Finite Element Problems", Int. J. num. Meth. Engrg. 12, 1677-1696 (1978).
10. E. Riks, "An Incremental Approach to the Solution of Snapping and Buckling Problems", Int. J. Solids Structures, 15, 529-551 (1979).
11. M. A. Crisfield, "Incremental/Iterative Solution Procedures for Nonlinear Structural Analysis", Int. Conf. on Numerical Methods for Nonlinear Problems Swansea, (1980).

12. M. A. Crisfield, "A Fast Incremental/Iterative Procedure that Handles SNAP-Through", *Comp. Struct.* 13, 55-62, (1981).
13. A. Noor, "Survey of Computer Programs for Solution of Nonlinear Structural and Solid Mechanics Problems", *Comp. Struct.* 13, 425-465, (1981).
14. J. Padovan, "Self Adaptive Incremental Newton-Raphson Algorithms", *Symposium on Computational Methods in Nonlinear Structural and Solid Mechanics*, Washington, D. C., (1980) also NASA (P-2147).
15. O. C. Zienkiewicz, "The Finite Element Method," McGraw-Hill Book Co., New York, (1977).
16. H. Matthies and G. Strang, "The Solution of Nonlinear Finite Element Equations", *Int. J. num. Meth. Engrg.* 14, 1613-1626 (1979).
17. T. J. R. Hughes, "Implicit-Explicit Finite Element Techniques for Symmetric and Nonsymmetric Systems," *Int. Conf. on Numerical Methods for Nonlinear Problem Swansea* (1980).
18. J. E. Dennis, Jr. and J. J. More, "Quasi-Newton Methods, Motivation and Theory," *Siam Review*, 19, 46-89 (1977).
19. J. L. Batoz, and G. Dhatt, "Incremental Displacement Algorithms for Nonlinear Problems", *Int. J. num. Meth. Engrg.*, 1262-1267, (1977).
20. P. Shariffi and E. P. Popov, "Nonlinear Buckling Analysis of Sandwich Arches", *J. Engrg. Mech. Div., ASCE*, 97, 1397-1412 (1971).
21. Y. C. Fung, "Foundations of Solid Mechanics", Prentice-Hall Inc., Englewood Cliffs, New Jersey (1965).
22. K. J. Bathe and A. P. Cimento, "Some Practical Procedures for the Solution of Nonlinear Finite Element Equations", *Comp. Meth. Appl. Mech. Engrg.* 22, 59-85 (1980).
23. F. B. Hildebrand, "Finite-Difference Equations and Simulations," Prentice-Hall Inc. Englewood Cliffs, New Jersey, (1968).
24. G. Broyden, "A Class of Methods for Solving Nonlinear Simultaneous Equations", *Math. Comp.* 19, 577-593, (1965).
25. R. Fletcher and M. J. D. Powell, "A Rapidly Convergent Descent Method for Minimization", *Comp. J.* 6, 163-168 (1963).
26. Huang, H. Y., "Unified Approach to Quadratically Convergent Algorithms for Function Minimization", *J. Optimization Theory Appl.* 5, 405-423, (1970).

References Con't

27. K. J. Bathe, "ADINA: A Finite Element Program for Automatic Dynamic Incremental Nonlinear Analysis", Report No. 82448-1 Acoustics and Vibrations Lab, Mech. Engrg. Dept. MIT, Cam. Mars (revised, 1978).
28. R. H. Iding, "Identification of Nonlinear Materials by Finite Methods", SESM Report No. 73-4, Dept. of Civ. Engrg., Univ. Cal, Berbeley (1973).
29. R. H. Mallett, L. Berke, "Automated Method for the Large Deflection and Instability Analysis of Three-Dimensional Truss and Frame Assemblies", Technical Report AFFDL-TR-66-102 Dec. (1966).
30. A. Gjelsuih, S. R. Bodner, "The Energy Criterion and Snap Buckling of Arches", J. of the Engrg. Mechanics, ASCE, 88, Oct. (1962).

Nomenclature

Abbreviation	Meaning
BFGS	Broyden-Fletcher-Goldfarb-Shanno update
DFP	Davidon, Fletcher, Powell method
CINR	Constrained Incremental Newton Raphson Method
CMINR	Constrained modified Incremental Newton Raphson Method
FE	Finite Element
HECS	Hyper ellipsoidal constraint surface
GP	General Purpose
ID	Indefinite
INR	Incremental Newton Raphson
MDID	Monotone decreasing indefinite
MDPD	Monotone decreasing positive definite
MIID	Monotone increasing indefinite
MIPD	Monotone increasing positive definite
MINR	Modified Incremental Newton Raphson
PD	Positive definite



# Nomenclature

Symbol	Meaning
$a_{\ell}^{i-1}$	Intercept of MINR extrapolation solution curve in $  \tilde{y}  , \lambda   \Delta\tilde{F}  $
$[B]$	Linearmatrix coefficient of $\tilde{y}$ defining strain
$[B_n(\tilde{y})] [G]$	Nonlinear matrix coefficient of $\tilde{y}$ defining strain
$[B^*(\tilde{y})]$	Matrix coefficient of $\tilde{y}$ defining variation in strain
$b_{\ell}$	Slope of MINR extrapolation of solution curve in $  \tilde{y}  , \lambda   \Delta\tilde{F}_{\ell}  $ space
$c_{\ell}$	Curvature parameter
$[D_T]$	Material stiffness
$e_R$	Allowable energy ratio
$\Delta E_{\ell}$	Energy Increment
$\tilde{F}_{\ell}$	Nodal force
$\Delta\tilde{F}_{\ell}$	Increment in nodal force
$\tilde{f}_{\ell}, \tilde{f}_{\ell}^i$	Load excursions relative to starting point of given increment
$[K_T(\tilde{y})], [K_T]$	Tangent stiffness
$K_u^{\ell i}$	Update parameter
$L_{ij}, \tilde{L}$	Lagrangian strain tensor
$[N]$	Shape function
$N_s$	Normed quantity use to define $\mu_{\ell}$
$O( )$	On the order of ( )
$Q_i, \tilde{Q}$	Body force
$R$	Initial region occupied by structure
$S_{ij}, \tilde{S}$	2nd Piola Kirchhoff stress tensor

Symbol	Meaning
$d\tilde{S}$	Increment in $\tilde{S}$
$u_i, \tilde{u}$	Cartesian type Lagrangian displacement
$v$	Volume
$\tilde{y}, \tilde{y}_\ell$	Nodal displacement
$\Delta \tilde{y}_\ell^i$	Increment in $\tilde{y}$
$\tilde{y}_\ell$	Displacement excursion relative to starting point of given increment
$[ ]$	Matrix
$(\sim)$	Vector
$   $	Absolute value
$       _1$	Absolute value norm
$       _2$	Euclidean norm
$[ ]^T, ( )^T$	transposition
$\delta( )$	Variational operator
$\lambda_\ell, \lambda_\ell^i$	Scaling parameter for load increment
$\chi_\ell^i$	Scaling parameter for energy increment

## DISTRIBUTION LIST FOR TOPICAL REPORT

NASA CR-165410

53

SELF-ADAPTIVE PREDICTOR-CORRECTOR ALGORITHMS FOR STATIC NONLINEAR  
STRUCTURAL ANALYSIS

GRANT NAG3-54

	<u>Mail Stop</u>	<u>Copies</u>
NASA Lewis Research Center		
21000 Brookpark Road		
Cleveland, OH 44135		
Attn: Contracting Officer	500-312	1
Technical Report Control Officer	5-5	1
Technology Utilization Office	3-16	1
AFSC Liaison Office	501-3	1
S&MT Division Contract File	49-6	2
Library	60-3	1
L. Berke	49-6	1
R. H. Johns	49-6	1
L. J. Kiraly	49-6	1
C. C. Chamis	49-6	7
M. S. Hirschbein	49-6	1
J. A. Ziemianski	49-6	1
J. D. McAleese	49-6	1
L. P. Ludwig	23-2	1
D. P. Fleming	23-2	1
A. F. Kascak	23-2	1
G. V. Brown	49-6	1
M. H. Tang	49-6	1
		1
National Aeronautics & Space Administration		
Washington, DC 20546		
Attn: NHS-22/Library		1
RTM-6/L. A. Harris		1
RTM-6/D. J. Weidman		1
NASA-Ames Research Center		
Moffett Field, CA 94035		
Attn: Library	202-3	1
NASA-Goddard Space Flight Center		
Greenbelt, MD 20771		
Attn: 252/Library		1
NASA-John F. Kennedy Space Center		
Kennedy Space Center, FL 32931		
Attn: Library	AD-CSO-1	1
NASA Langley Research Center		
Hampton, VA 23665		
Attn: Library	185	1
M. F. Card	244	1
M. M. Mikulas	190	1

	<u>Mail Stop</u>	<u>Copies</u>
NASA-Lyndon B. Johnson Space Center Houston, TX 77001 Attn: JM6/Library		1
NASA-George C. Marshall Space Flight Center Marshall Space Flight Center, AL 35812 Attn: AS61/Library		1
Jet Propulsion Laboratory 4800 Oak Grove Drive Pasadena, CA 91103 Attn: Library B. Wada R. Levi		1 1 1
NASA S&T Information Facility P.O. Box 8757 Baltimore-Washington Int. Airport, MD 21240 Attn: Acquisition Department		10
Air Force Aeronautical Propulsion Laboratory Wright Patterson AFB, OH 45433 Attn: Z. Gershon E. Bailey		1 1
Air Force Systems Command Aeronautical Systems Division Wright-Patterson AFB, OH 45433 Attn: Library C. W. Cowie J. McBane		1 1 1
Aerospace Corporation 2400 E. El Segundo Blvd. Los Angeles, CA 90045 Attn: Library-Documents		1
Air Force Office of Scientific Research Washington, DC 20333 Attn: A. K. Amos		1
Department of the Army U.S. Army Material Command Washington, DC 20315 Attn: AMCRD-RC		1
U.S. Army Ballistics Research Laboratory Aberdeen Proving Ground, MD 21005 Attn: Dr. Donald F. Haskell	DRXBR-BM	1
Mechanics Research Laboratory Army Materials & Mechanics Research Center Watertown, MA 02172 Attn: Dr. Donald W. Oplinger		1

	<u>Mail Stop</u>	<u>Copies</u>
U.S. Army Missile Command Redstone Scientific Information Center Redstone Arsenal, AL 35808 Attn: Document Section		1
AFFDL/FBE Wright-Patterson AFB, OH 45433 Attn: D. W. Smith		1
Commanding Officer U.S. Army Research Office (Durham) Box, CM, Duke Station Durham, NC 27706 Attn: Library		1
Bureau of Naval Weapons Department of the Navy Washington, DC 20360 Attn: RRRE-6		1
Commander U.S. Naval Ordnance Laboratory White Oak Silver Springs, MD 20910 Attn: Library		1
Director, Code 6180 U.S. Naval Research Laboratory Washington, DC 20390 Attn: Library		1
Denver Federal Center U.S. Bureau of Reclamation P.O. Box 25007 Denver, CO 80225 Attn: P. M. Lorenz		1
Naval Air Propulsion Test Center Aeronautical Engine Department Trenton, NJ 08628 Attn: Mr. James Salvino		1
Naval Air Propulsion Test Center Aeronautical Engine Department Trenton, NJ 08628 Attn: Mr. Robert DeLucia		1
Federal Aviation Administration Code ANE-214, Propulsion Section 12 New England Executive Park Burlington, MA 01803 Attn: Mr. Robert Berman		1

	<u>Mail Stop</u>	<u>Copies</u>
Federal Aviation Administration DOT Office of Aviation Safety, FOB 10A 800 Independence Ave., S.W. Washington, DC 20591 Attn: Mr. John H. Enders		1
FAA, ARD-520 2100 2nd Street, S.W. Washington, DC 20591 Attn: Commander John J. Shea		1
National Transportation Safety Board 800 Independence Ave., S.W. Washington, DC 20594 Attn: Mr. Edward P. Wizniak	TE-20	1
Arizona State University Department of Aerospace Engineering and Engineering Science Tempe, AZ 85281 Attn: H. D. Nelson		1
Rockwell International Corporation Los Angeles International Airport Los Angeles, CA 90009 Attn: Mr. Joseph Gausselin	D 422/402 AB71	1
Rensselaer Polytechnic Institute Troy, NY 12181 Attn: R. Loewy		1
Cleveland State University Department of Civil Engineering Cleveland, OH 44115 Attn: J. J. Tomko		1
M.I.T. Cambridge, MA 02139 Attn: K. Bathe		1
T. H. Pian		1
J. Mar		1
E. A. Witmer		1
J. Dugundji		1
University of Illinois at Chicago Circle Department of Materials Engineering Box 4348 Chicago, IL 60680 Attn: Dr. Robert L. Spilker		1

	<u>Mail Stop</u>	<u>Copies</u>
Detroit Diesel Allison General Motors Corporation Speed Code T3, Box 894 Indianapolis, IN 46206 Attn: Mr. William Springer Mr. J. Byrd		1 1
General Motors Corporation Warren, MI 48090 Attn: R. J. Trippet		1
AVCO Lycoming Division 550 South Main Street Stratford, CT 06497 Attn: Mr. Herbert Kaehler		1
Beech Aircraft Corporation, Plant 1 Wichita, KA 67201 Attn: Mr. M. K. O'Connor		1
Bell Aerospace P.O. Box 1 Buffalo, NY 14240 Attn: G. C. C. Smith		1
Boeing Aerospace Company Impact Mechanics Lab P.O. Box 3999 Seattle, WA 98124 Attn: Dr. R. J. Bristow		1
Boeing Commercial Airplane Company P.O. Box 3707 Seattle, WA 98124 Attn: Dr. Ralph B. McCormick		1
Boeing Commercial Airplane Company P.O. Box 3707 Seattle, WA 98124 Attn: Mr. David T. Powell	73-01	1
Boeing Commercial Airplane Company P.O. Box 3707 Seattle, WA 98124 Attn: Dr. John H. Gerstle		1
Boeing Company Wichita, KA Attn: Mr. C. F. Tiffany		1

	<u>Mail Stop</u>	<u>Copies</u>
McDonnell Douglas Aircraft Corporation P.O. Box 516 Lambert Field, MO 63166 Attn: Library		1
Douglas Aircraft Company 3855 Lakewood Blvd. Long Beach, CA 90846 Attn: Mr. M. A. O'Connor, Jr.	36-41	1
Garrett AiResearch Manufacturing Co. 111 S. 34th Street P.O. Box 5217 Phoenix, AZ 85010 Attn: L. A. Matsch		1
General Dynamics P.O. Box 748 Fort Worth, TX 76101 Attn: Library		1
General Dynamics/Convair Aerospace P.O. Box 1128 San Diego, CA 92112 Attn: Library		1
General Electric Company Interstate 75, Bldg. 500 Cincinnati, OH 45215 Attn: Dr. L. Beitch	K221	1
Dr. M. Roberts	K221	
Dr. V. Gallardo	K221	1
General Electric Company Aircraft Engine Group Lynn, MA 01902 Attn: Mr. Herbert Garten		1
Grumman Aircraft Engineering Corp. Bethpage, Long Island, NY 11714 Attn: Library		1
H. A. Armen		1
IIT Research Institute Technology Center Chicago, IL 60616 Attn: Library		1
Lockheed California Company P.O. Box 551 Dept. 73-31, Bldg. 90, PL. A-1 Burbank, CA 91520 Attn: Mr. D. T. Pland		1



Mail StopCopies

Lockheed California Company  
 P.O. Box 551  
 Dept. 75-71, Bldg. 63, PL. A-1  
 Burbank, CA 91520  
 Attn: Mr. Jack E. Wignot

1

Northrop Space Laboratories  
 3401 West Broadway  
 Hawthorne, CA 90250  
 Attn: Library

1

North American Rockwell, Inc.  
 Rocketdyne Division  
 6633 Canoga Avenue  
 Canoga Park, CA 91304  
 Attn: Library, Dept. 596-306

1

North American Rockwell, Inc.  
 Space & Information Systems Division  
 12214 Lakewood Blvd.  
 Downey, CA 90241  
 Attn: Library

1

Norton Company  
 Industrial Ceramics Division  
 Armore & Spectramic Products  
 Worcester, MA 01606  
 Attn: Mr. George E. Buron

1

Norton Company  
 1 New Bond Street  
 Industrial Ceramics Division  
 Worcester, MA 01606  
 Attn: Mr. Paul B. Gardner

1

United Aircraft Corporation  
 Pratt & Whitney Group  
 Government Products Division  
 P.O. Box B2691  
 West Palm Beach, FL 33402  
 Attn: Library  
       R. A. Marmol

1

1

United Aircraft Corporation  
 Pratt & Whitney Aircraft Group  
 400 Main Street  
 East Hartford, CT 06108  
 Attn: Library  
       R. Liss  
       D. H. Hibner  
       C. Platt

1

1

1

1

	<u>Mail Stop</u>	<u>Copies</u>
United Aircraft Corporation Hamilton Standard Division Windsor Locks, CT 06096 Attn: Dr. G. P. Townsend Dr. R. A. Cornell		1 1
Aeronautical Research Association of Princeton, Inc. P.O. Box 2229 Princeton, NJ 08540 Attn: Dr. Thomas McDonough		1
Republic Aviation Fairchild Hiller Corporation Farmington, Long Island, NY Attn: Library		1
Rohr Industries Foot of H Street Chula Vista, CA 92010 Attn: Mr. John Meaney		1
TWA, Inc. Kansas City International Airport P.O. Box 20126 Kansas City, MO 64195 Attn: Mr. John J. Morelli		1
Stevens Institute of Technology Castle Point Station Hoboken, NJ 07030 Attn: F. Sisto A. T. Chang		1 1
Mechanical Technologies Inc. Latham, NY Attn: M. S. Darlow		1
Shaker Research Corporation Northway 10, Executive Park Ballston Lake, NY 12019 Attn: L. Lagace		1
Lockheed Palo Alto Research Labs Palo Alto, CA 94304 Attn: B. O. Almroth		1
Lockheed Missiles and Space Company Huntsville Research & Engineering Center P.O. Box 1103 Huntsville, AL 35894 Attn: H. B. Shirley		1

	<u>Mail Stop</u>	<u>Copies</u>
MacNeal-Schwendler Corporation 7442 North Figueroa Street Los Angeles, CA 90041 Attn: R. H. MacNeal		1
MARC Analysis Research Corporation 260 Sheridan Avenue, Suite 314 Palo Alto, CA 94306 Attn: P. V. Marcel		1
United Technologies Research Center East Hartford, CT 06108 Attn: Dr. A. Dennis		1
Georgia Institute of Technology School of Civil Engineering Atlanta, GA 30332 Attn: S. N. Atluri		1
Georgia Institute of Technology 225 North Avenue Atlanta, GA 30332 Attn: G. J. Simitsis		1
Lawrence Livermore Laboratory P.O. Box 808, L-421 Livermore, CA 94550 Attn: M. L. Wilkins		1
Lehigh University Institute of Fracture and Solid Mechanics Bethlehem, PA 18015 Attn: G. T. McAllister		1
Materials Science Corporation 1777 Walton Road Blue Bell, PA 19422 Attn: W. B. Rosen		1
National Bureau of Standards Engineering Mechanics Section Washington, DC 20234 Attn: R. Mitchell		1
Purdue University School of Aeronautics & Astronautics West Lafayette, IN 47907 Attn: C. T. Sun		1
University of Dayton Research Institute Dayton, OH 45409 Attn: F. K. Bogner		1

	<u>Mail Stop</u>	<u>Copies</u>
Texas A&M University Aerospace Engineering Department College Station, TX 77843 Attn: W. E. Haisler J. M. Vance		1 1
V. P. I. and State University Department of Engineering Mechanics Blacksburg, VA 24061 Attn: R. H. Heller		1
University of Arizona College of Engineering Tucson, AZ 87521 Attn: R. H. Gallagher J. C. Heinrich		1 1
University of California Department of Civil Engineering Berkeley, CA 94720 Attn: E. Wilson		1
University of Kansas School of Engineering Lawrence, KS 66045 Attn: R. H. Dodds		1
University of Virginia School of Engineering & Applied Science Charlottesville, VA 22901 Attn: E. J. Gunter		1

**End of Document**